NEW APPROACH FOR PRODUCTION ANALYSIS OF SHALE GAS/OIL RESERVOIRS

A Thesis

by

VISHAL KUMAR SHARMA

Submitted to the Office of Graduate and Professional Studies of
Texas A&M University
in partial fulfillment of the requirements for the degree of

MASTER OF SCIENCE

Chair of Committee,	Michael J. King
Co-Chair of Committee,	Akhil Datta-Gupta
Committee Member,	Yalchin Efendiev
Head of Department,	Dan Hill

May 2016

Major Subject: Petroleum Engineering

ABSTRACT

Shale Gas/Oil reservoirs have emerged as an important reserve in global energy markets in the last decade. Oil and gas production from shales has been possible due to horizontal drilling and multiple-stage fracturing.

Shale has low permeability, in the range of nano-darcy's. To increase flow from such reservoirs the only known solution is to increase the area for flow, which can be done by Hydraulic Fracturing. This gives an optimum solution for economically producing hydrocarbon from these reservoirs.

It is very important to find a way to quantify reservoir and fracture permeability, and the extent of the hydraulic fractures that have been created.

In this research, the focus is on a method of analysis which can give information on the propagation of pressure waves as well as on the properties of the reservoir. These techniques gives us two approaches. In the first, the reservoir and fracture model is fixed and the pressure wave propagation and the reservoir performance is predicted. In the second approach, performance is measured and then inverted for the area of the propagating pressure wave. This interpretation technique does not involve any assumed model but is developed directly from production data.

The current research approach is based on the concept of the diffusive time of flight and drainage volumes. The diffusive time of flight is derived from the high frequency asymptotic limit of the diffusivity equation.

For the first approach, we have assumed different wave propagation geometries. Analytical solution for these geometries were validated with synthetic simulation case and by comparing it with other well testing equations.

The second approach is a novel method of interpretation of performance data in which we try to evaluate a model without using any pre-assumed geometry of the fracture or pressure wave propagation. This approach gives the new way to interpret field data and to compare the well performance based on the propagation area.

Our second approach for the analysis of the production data is more promising than other approach as the requirement for the predefined model was eliminated.

DEDICATION

To my parents

For their support and love.

.

ACKNOWLEDGEMENTS

First and foremost, I would like to thank my committee chair, Dr. Michael J. King, who has given me the opportunity to work with him. I would also like to thank him for guiding me throughout my research and encouraging me to explore new ideas.

I would like to thank Co-Chair, Dr. Akhil Datta-Gupta and Committee member, Dr. Yalchin Efendiev, for their guidance and support during the course of research.

During this work, I have worked and learned a lot from the other students of the MCERI research group. It was their help which made me learn and apply different ideas more efficiently. I would also like to thank MCERI for funding this research work.

During my Master's coursework, I have learned a lot from different faculty members. I would like to thank all the professors who taught me during my Master's degree at Texas A&M University.

NOMENCLATURE

r	Radius of investigation
k	Permeability
t	Time
ϕ	Porosity
c_t	Total compressibility
μ	Fluid viscosity
τ	Diffusive time of flight
u	Darcy's velocity
$V_p(t)$	Drainage volume
$V_p(\tau)$	Pore volume contained within a τ contour
$w(\tau)$	Derivative of pore volume with respect to τ
q	Flux
p	Pressure
IRR	Instantaneous Recovery Ratio
q_w	Flux through well
r_w	Wellbore radius
x,y	Variables for Cartesian coordinate system
ξ, η	Variables for Elliptical coordinate system
L	Fracture half length
p_D	Dimensionless pressure

α	Diffusivity
x_f	Fracture half length
h	Thickness of reservoir
t_{L_fD}	Dimensionless time
p_{wf}	Bottom hole pressure
p_i	Initial pressure
$W_p(t)$	Cumulative production
ρ	Density of fluid
g	Acceleration of gravity
f_f	Friction factor
$V_{liq,res}$	Total fluid volume
$V_{o,res}$	Oil volume
$V_{g,res}$	Gas volume
$V_{w,res}$	Water volume
B_o	Formation volume factor, oil
B_w	Formation volume factor, water
B_g	Formation volume factor, gas
R_s	Gas oil ratio
N_{Re}	Reynolds number

TABLE OF CONTENTS

Page

LIST OF FIGURES

Page

LIST OF TABLES

Page

1. INTRODUCTION

Unconventional Shale gas/oil reservoirs have become an important reserve for the US energy supplies. The production is mainly because of the advanced technology in the horizontal well completion.

Unconventional Shale gas/oil reservoirs are characterized by very low permeability (nano-darcy). Techniques such as decline curve analysis [4-6] and pressure/rate transient analysis [7-9] are generally applied for the reserve and property estimation. Even though these techniques are easy to apply, they have limitations of homogeneous media and simple systems assumptions.

The research presented here is based on the asymptotic limit of the diffusivity equation for impulse source/sink [10, 11]. Resulting Eikonal equation gives the relationship between the spatial coordinate DTOF and diffusivity.

The relationship between the spatial distribution of drainage volume $V_p(\tau)$ and drainage volume propagation with time $V_p(t)$ could be established [12].This relationship could be used to get the analytical formulation of drainage volume $V_p(t)$. The only limitation is that we must know the geometry of the drainage volume in the spatial coordinate as input to the calculation, i.e. $V_p(\tau)$.

When talking about our novel method for the analysis of production data, the relationship of $V_p(\tau)$ and $V_p(t)$ is very important. The drainage volume, $V_p(t)$, can be directly calculated from the production data. The relationship between the two allows us to invert for the

drainage volume, $V_p(t)$, to calculate the derivative of $V_p(\tau)$ with τ, which is proportional to the cross-sectional area of the pressure wave in the reservoir. This inversion technique is novel and basically gives us an idea of the spatial distribution of the drainage volume in τ. Thus this method gives the spatial distribution of drainage volume merely from the production data of the well, which in turn gives the idea of the hydraulic fracture effectiveness and reservoir properties.

Here this research work will be focused into two parts. First is the development of analytical formulation of the drainage volume by assuming pressure wave propagation geometry for homogeneous reservoir, which is based on fracture models. Second is the development of the method for analysis of the production data to get the derivative of $V_p(\tau)$ with τ, which is a model free analysis.

2. LITERATURE REVIEW

This section contains the literature review in the following pattern. First part will give the overview of the methodology. Second part will give the overview of the approach for the analytical solution of the diffusivity equation for infinite conductivity fracture.

2.1 Methodology

2.1.1 Diffusive time of flight

Lee [13] defined the radius of investigation as the distance of peak pressure disturbance from an impulse source or sink.

Figure 1 Wave front propagation[14]

For a 2D homogeneous reservoir,

$$r = \sqrt{\frac{kt}{948\phi\mu c_t}} \tag{1}$$

The Diffusive Time of Flight (DTOF), τ, is derived from the high frequency asymptotic limit of the diffusivity equation for heterogeneous porous media [10, 11].

The asymptotic limit of the diffusivity equation leads to the Eikonal equation which is[15]:

$$\nabla \tau(\vec{x}) \cdot \overline{\overline{k}}(\vec{x}) \cdot \nabla \tau(\vec{x}) = \phi(\vec{x}) \mu c_t \tag{2}$$

The variable $\tau(\vec{x})$ is associated with the propagation of the peak of the pressure pulse for an impulse source. This mathematical statement is for a full tensor permeability, while isotropic media with scalar permeability is more frequently used. For the isotropic case with scalar permeability, Eikonal equation relates incremental τ to distance in the following finite differential formula.

$$\delta\tau = \sqrt{\frac{\phi \mu c_t}{k}} \cdot \delta r \tag{3}$$

2.1.2 Diffusivity and $w(\tau)$ formulation

The starting point of our methodology is the diffusivity equation in heterogeneous porous media [10, 11, 16].

Diffusivity equation can be written in terms of pressure and Darcy velocity (for slightly compressible fluids)

$$\varphi(\vec{x}) c_t \frac{\partial p(\vec{x}, t)}{\partial t} + \nabla \cdot \vec{u} = 0 \tag{4}$$

Where,

$$\vec{u} = -\frac{1}{\mu} \vec{\vec{k}}(\vec{x}) \cdot \nabla p \tag{5}$$

Above equation can be written in 1D by coordinate transformation .

$$\frac{\partial p}{\partial t} - \frac{1}{w(\tau)} \frac{\partial}{\partial \tau}\left(w(\tau) \frac{\partial p}{\partial \tau} \right) = 0 \tag{6}$$

Where,

$$w(\tau) = \frac{dV_p(\tau)}{d\tau} \tag{7}$$

Here w(τ) is the differential of the drainage volume which implies that it is related to the surface area of the drainage volume. Also it is a function of τ, which indicates that it is related to the geometry of the drainage volume. This 1D diffusivity equation includes the heterogeneity and the physical properties in w(τ). This relationship is very important as it relates the pressure, rate and drainage volume.

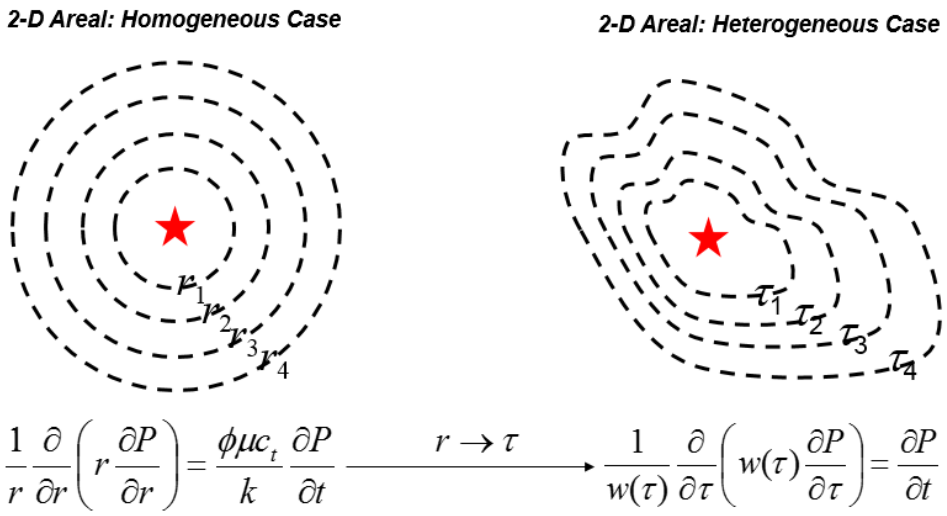

Figure 2. Analogy between the w(τ) formulation in heterogeneous reservoirs and the circular drainage volume in a homogeneous reservoir [15]

2.1.3 Asymptotic solution to the diffusivity equation

The exposition presented in this section closely follows what was presented in Yang, C., et al (2015).

Diffusivity equation for slightly compressible fluid can be transformed in terms DTOF, τ, by coordinate transformation to obtain single dimensional diffusivity equation (Eq.(8))[16].

$$\frac{\partial p}{\partial t} - \frac{1}{w(\tau)} \frac{\partial}{\partial \tau} \left(w(\tau) \frac{\partial p}{\partial \tau} \right) = 0 \tag{8}$$

Total flux over a τ contour can be calculated by writing the Darcy's law in τ coordinate system (Eq. (9).

$$q = c_t w(\tau) \frac{\partial p}{\partial \tau} \tag{9}$$

We can write the diffusivity equation in terms of total flux (Eq.(10)).

$$\frac{\partial q}{\partial t} - w(\tau) \frac{\partial}{\partial \tau} \left(\frac{1}{w(\tau)} \frac{\partial q}{\partial \tau} \right) = 0 \tag{10}$$

For a fixed flow rate drawdown in an infinite domain, the initial and boundary conditions are

$$\begin{array}{lll} t = 0 & p = p_{init} & q = 0 \\ \tau = 0 & & q = q_w \\ \tau \to \infty & p \to p_{init} & q \to 0 \end{array} \tag{11}$$

Well is specified at $\tau = 0$, which may be at $r = 0$, for fault surface or for the line source approximation, or at a finite wellbore radius, r_w. For our case at $\tau = 0$ we have the boundary of a single infinite conductivity fracture.

w(τ) is derivative of pore volume with spatial coordinate (τ), it is the wave propagation surface area. We can consider w(τ) as power-law in τ (linear, radial and spherical cases) and it will include all solution for diffusivity equation. Our equations are linear in flux and pressure and dimensional analysis tells that dimensionless flux function will depends on the ratios of τ and t.

We can work with Boltzmann variable (ξ).

$$\xi = \frac{\tau^2}{4t} \tag{12}$$

Now,

$$\frac{\partial q}{\partial \tau} = \frac{\tau}{2t}\frac{dq}{d\xi} \tag{13}$$

$$\frac{\partial q}{\partial t} = -\frac{\tau^2}{4t^2}\frac{dq}{d\xi} = -\frac{\tau^2}{4t^2}\frac{2t}{\tau}\frac{\partial q}{\partial \tau} = -\frac{\tau}{2t}\frac{\partial q}{\partial \tau} \tag{14}$$

Hence from diffusivity equation we have

$$\frac{\tau}{2t}\left(\frac{1}{w(\tau)}\frac{dq}{d\tau}\right) + \frac{\partial}{\partial \tau}\left(\frac{1}{w(\tau)}\frac{dq}{d\tau}\right) = 0 \tag{15}$$

On integration

$$\frac{1}{w(\tau)}\frac{dq}{d\tau} = -\frac{q_w}{V_p(t)}e^{-\frac{\tau^2}{4t}} \tag{16}$$

Flux, $q(\tau, t)$, and the drainage volume, $V_p(t)$, depend upon $w(\tau)$. On integration we get the flux.

$$q(\tau,t) = \frac{q_w}{V_p(t)}\int_0^\infty d\tau.w(\tau).e^{-\frac{\tau^2}{4t}} = \frac{q_w}{V_p(t)}\int_0^\infty dV_p(\tau).e^{-\frac{\tau^2}{4t}} \tag{17}$$

Now, $V_p(t)$, for τ=0 is calculated for $q(\tau, t) = q_w$ as is determined from the boundary condition at τ=0.

$$V_p(t) = \int_0^\infty dV_p(\tau).e^{-\frac{\tau^2}{4t}} = \int_0^\infty w(\tau)e^{-\frac{\tau^2}{4t}}d\tau \tag{18}$$

The last equation is one of the most important equations which will be used for finding analytical solution for the drainage volume and for the production data analysis.

2.2 Solution to diffusivity equation for infinite conductivity fracture

Solutions for the diffusivity equation for an infinite conductivity fracture are not new. There has been a lot of work which has been done for the diffusivity equation solution for fracture system. Diffusivity equation can be solved numerically in Cartesian system with the use of different numerical techniques i.e. finite difference, finite element etc. Here the main focus of the literature review are the analytical solutions for the same.

Fracture in a low permeability matrix acts as a highway where the flow of the hydrocarbon takes place. Hydrocarbon flows into the fracture from the reservoir rock and from there it

flows to the well if the fracture is connected to the well. The flow inside the fracture is considered with no restrictions, an assumption for infinite conductivity.

Most of the models assumed for the derivation for single infinite conductivity fracture is based on the fact that a surface is created by the slitting of the rock in rectangular shape to reservoir rock and has infinite flow capacity within it [13, 17-21].

When the flow in the fracture starts different flow patterns take place. Initially it acts as formation linear flow with most of the flow is in the fracture directly from the surface. In the later stage once the pressure wave starts moving into the reservoir, the flow transitions to elliptical in nature. For very late time the flow is radial. Fig. 3 shows the different flow types.

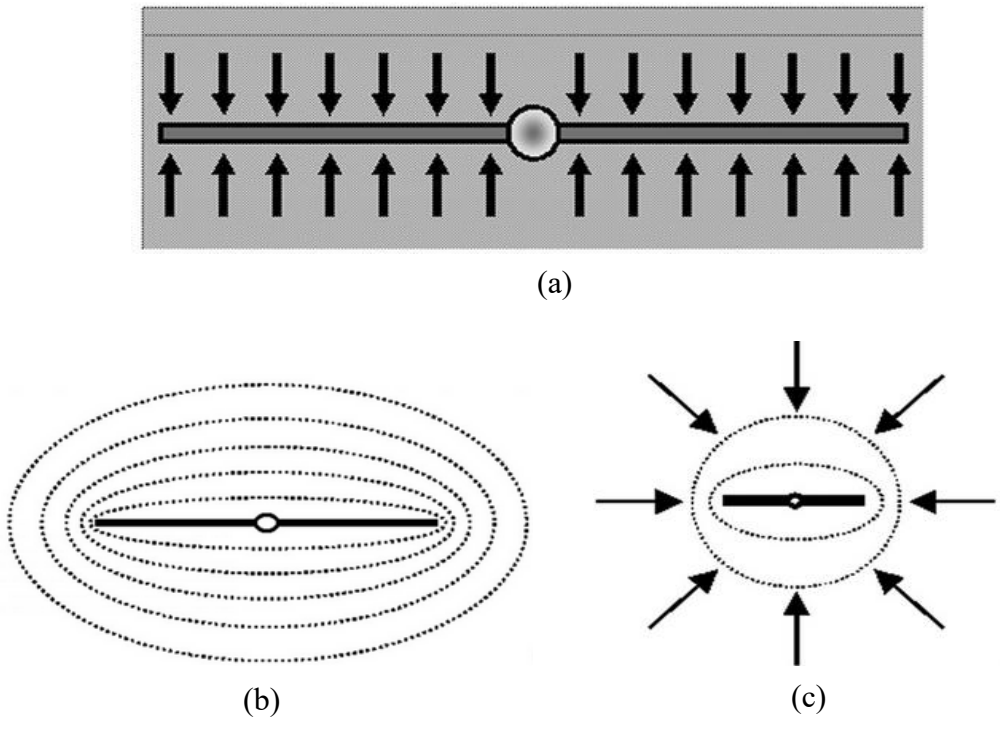

Figure 3 (a) Linear flow regime (b) Elliptical flow (c) Radial flow[1]

Although our discussion is solely for infinite conductivity fracture but for finite conductivity fracture we will see fracture linear and bilinear flow pattern before formation linear flow.

For solving the diffusivity equation for fracture system elliptical coordinate system is used [3, 20, 22]. The same method is used while solving for a horizontal well of infinite conductivity or for elliptical bounded reservoirs [23-25].

In almost all the literature available for elliptical flow system, first the diffusivity equation is transformed into the elliptical coordinate system i.e. the Cartesian system is transformed into the sets of hyperbolas and ellipses. Now these equations are solved using Laplace transformation and the method of separation of variables. With this method we reached to a solution in Laplace Space and that to a series functions called Mathieu Functions. This solution in Laplace Space could be reversed back by using a numerical inversion techniques like Stehfest [26].

A summary for the solution of the diffusivity equation for an infinite conductivity fracture is summarized below.

For single phase, slightly compressible fluid

Diffusivity Equation:

$$\nabla^2 p = \frac{\phi \mu c_t}{k} \frac{\partial p}{\partial t} \tag{19}$$

In a Cartesian coordinate system:

$$\frac{\partial^2 p}{\partial x^2}+\frac{\partial^2 p}{\partial y^2}=\frac{\phi\mu c_t}{k}\frac{\partial p}{\partial t} \tag{20}$$

Elliptical Coordinates Transformation

$$\begin{aligned} x&=L.\cosh\xi.\cos\eta \\ y&=L.\sinh\xi.\sin\eta \end{aligned} \tag{21}$$

Here L is the fracture half length.

Elliptical coordinate system is the series of the confocal hyperbolas and ellipses which are normal to each other.

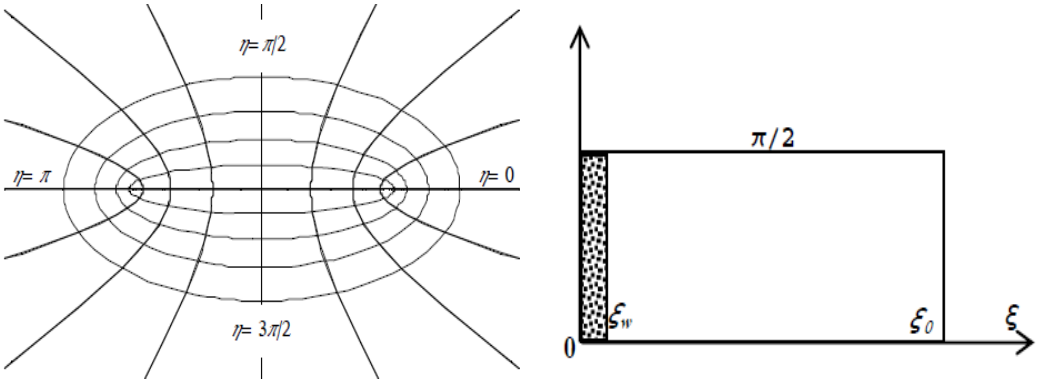

Figure 4 Elliptical coordinates and elliptical system after transformation[3]

$$\begin{aligned} &\text{Ellipse Eqn, } \left(\frac{x}{L\cosh\xi}\right)^2+\left(\frac{y}{L\sinh\xi}\right)^2=1 \\ &\text{Hyperbola Eqn, } \left(\frac{x}{L\cos\eta}\right)^2-\left(\frac{y}{L\sin\eta}\right)^2=1 \end{aligned} \tag{22}$$

Cartesian form of diffusivity equation is transformed in terms of elliptical coordinate system (Eq.(23)).

$$\frac{\partial^2 p}{\partial \xi^2}+\frac{\partial^2 p}{\partial \eta^2}=\frac{\varphi \mu c_t L^2}{2k}\left[\cosh(2\xi)-\cos(2\eta)\right]\frac{\partial p}{\partial t} \tag{23}$$

The Laplace transform is taken for Eq.(23) with dimensionless variables and the method of separation of variables is applied as shown in Eq.(24),(25). We get the set of equations Eq.(26),(27). These equations have series solution in the form of Mathieu Function [3, 24]. Following is the summary of the equations.

$$\frac{\partial^2 \bar{p}_D}{\partial \xi^2}+\frac{\partial^2 \bar{p}_D}{\partial \eta^2}=\frac{s}{2}\left[\cosh(2\xi)-\cos(2\eta)\right]\bar{p}_D \tag{24}$$

$$\bar{p}_D(\xi,\eta)=X(\xi).H(\eta) \tag{25}$$

$$\frac{\partial^2 H}{\partial \eta^2}+(a+\frac{s}{2}\cos(2\eta))H \tag{26}$$

$$\frac{\partial^2 X}{\partial \xi^2}-(a+\frac{s}{2}\cosh(2\xi))X \tag{27}$$

Our main concern is to use the Eq.(23) from this development and to combine our methodology of the diffusive time of flight to find the analytical solution for the drainage volume.

3. ANALYTICAL SOLUTION FOR THE DRAINAGE VOLUME FOR INFINITE CONDUCTIVITY FRACTURE

As indicated in the literature review, the current research is concentrated into two parts. First part of the research will concentrate on the analytical solution of the drainage volume for an infinite conductivity fracture. The second part will be concentrated on the method of analysis of production data. Here we discuss the analytical solution for the drainage volume.

For the analytical solution of the drainage volume for the infinite conductivity fracture, our methodology using the Diffusive Time of Flight is applied to the earlier developed method for solution of the diffusivity equation for the infinite conductivity fracture.

3.1 Drainage volume for infinite conductivity fracture

Our starting point equation for the derivation of analytical solution for drainage volume is $V_p(t) = \int_0^\infty dV_p(\tau).e^{-\frac{\tau^2}{4t}} = \int_0^\infty w(\tau)e^{-\frac{\tau^2}{4t}}d\tau$ .The most important quantity that is needed for our derivation is the knowledge of $w(\tau) = \frac{dV_p(\tau)}{d\tau}$.$w(\tau)$ is the derivative of the drainage volume with respect to the diffusive time of flight. This quantity basically gives information on the geometry of pressure wave propagation. Here we are assuming that $w(\tau)$ inside the hydraulic fracture is 0 as fracture is infinite conductivity and the drainage volume is constant for the fracture cavity. The reason for this is that the pressure wave propagation in the infinite conductive fracture will be so fast that we can say that the

impulse disturbance is the same inside the fracture. Now the pressure wave propagation will start all around the fracture at the same time and starting point will be whole fracture boundary.

The initial value of the derivative of the drainage volume gives us the idea of the fracture area which has been created for the hydrocarbon flow. The assumption of a fracture as a simple rectangular shape is a simplified description of the overall surface area which has been created. We accommodate the whole geometry in a very simple model.

Different geometric shapes for the pressure wave propagation are assumed for the derivation of the solution. Derivations are shown in the following subsections for the different geometries.

3.1.1 Pill box model

Here we consider a fracture which is created vertically and is fully completed throughout the formation layer of the reservoir. The fracture is fully completed and is of infinite conductivity throughout. Here we have assumed the homogeneous reservoir throughout for the derivation of our model.

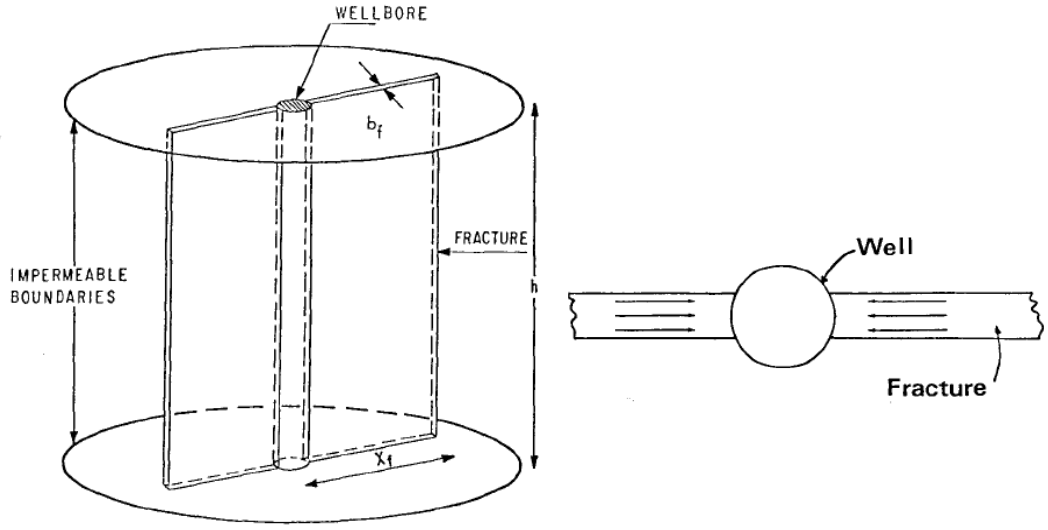

Figure 5 Lateral and top view of single fully completed fracture[2]

As we have assumed that the fracture is of the infinite conductivity, so throughout the fracture our Diffusive Time of Flight DTOF is zero.

As the production through well starts, we can assume that pressure wave will be traveling with the same speed as our diffusivity i.e.$\frac{k}{\phi\mu c_t}$ is same for the formation (homogeneous condition). So a pressure wave will be equidistant from the fracture whether it is the surface of the fracture or the end points of the fracture.

In the following Fig.6,7 the geometry assumption is shown clearly.

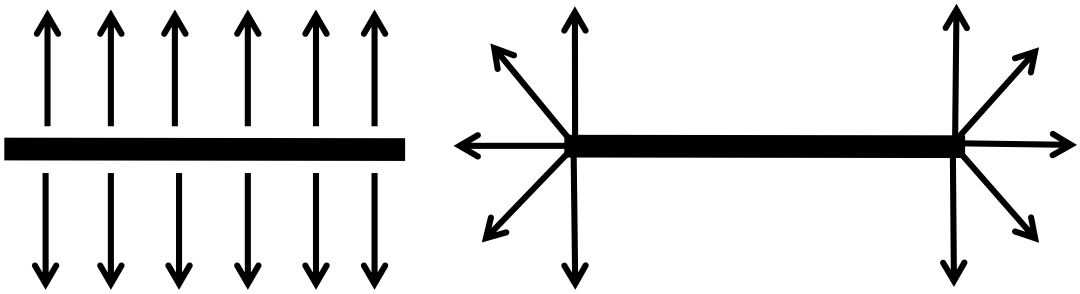

Figure 6 Lateral and Radial distance of the pressure front

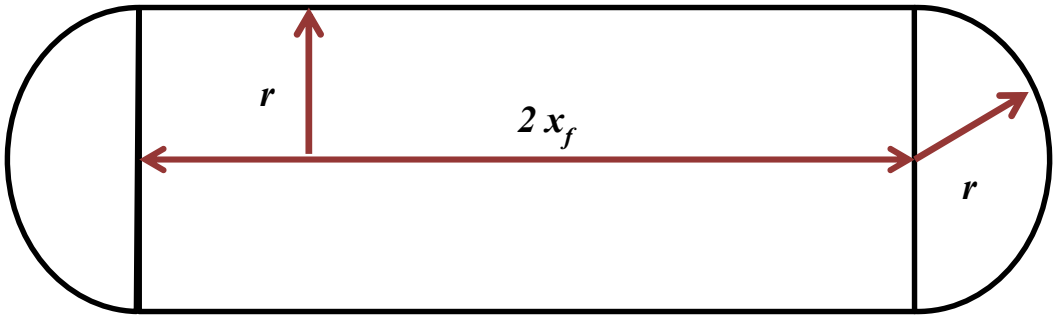

Figure 7 Geometry of pressure wave propagation for pill box Shape

Eikonal Equation (Eq.(2)), when written for isotropic case comes up as $\sqrt{\alpha(x)}|\nabla\tau| = 1$,

where $\alpha(x) = \dfrac{k}{\phi\mu c_t}$ or diffusivity.For homogeneous media, $\delta\tau = \sqrt{\dfrac{\phi\mu c_t}{k}} \cdot \delta r$

Integrated form: $\tau = \sqrt{\dfrac{\phi\mu c_t}{k}} \cdot r$ or $\sqrt{\alpha} \cdot \tau = r$

Now, for this geometry

$$V_p(r) = (\pi r^2 + 4x_f r).h.\phi \tag{28}$$

Now substituting $\sqrt{\alpha} \cdot \tau = r$

$$V_p(\tau) = (\pi\alpha\tau^2 + 4x_f\sqrt{\alpha}\tau).h.\phi \tag{29}$$

$$w(\tau) = \frac{dV_p(\tau)}{d\tau} = (2\pi\tau\alpha + 4x_f\sqrt{\alpha}).h.\phi \tag{30}$$

$$V_p(t) = \int_0^\infty dV_p(\tau).e^{-\frac{\tau^2}{4t}} = \int_0^\infty w(\tau)e^{-\frac{\tau^2}{4t}}d\tau = \int_0^\infty (2\pi\tau\alpha + 4x_f\sqrt{\alpha}).h.\phi.e^{-\frac{\tau^2}{4t}}d\tau$$

On integration,

$$V_p(t) = h.\phi.(4\pi.\alpha.t + 4x_f\sqrt{\pi.\alpha.t}) \tag{31}$$

$$V_p(t) = h.\phi.(\frac{4\pi}{\phi\mu c_t}.k.t + 4\sqrt{\frac{\pi}{\phi\mu c_t}}.(x_f.\sqrt{k}).\sqrt{t}) \tag{32}$$

Here, we have the final equation Eq.(32) for the drainage volume. The first part of the equation is linear with time and the other part of the equation is linear with square root time.

Here for the very small time the square root time terms are more influential and for the large value of time linear terms are more influential. Plot of the drainage volume versus time gives a half-slope for the early times and for the later times the slope is of unit value. The half slope in the drainage volume signifies the linear formation flow. The unit slope signifies the radial flow, which is at the later time.

The information that we get from these two parts of the plots is the coefficients $h.\frac{4\pi}{\mu c_t}.k$ from the unit slope part and $4.h.\sqrt{\frac{\pi\phi}{\mu c_t}}.(x_f.\sqrt{k})$ from the half slope part.

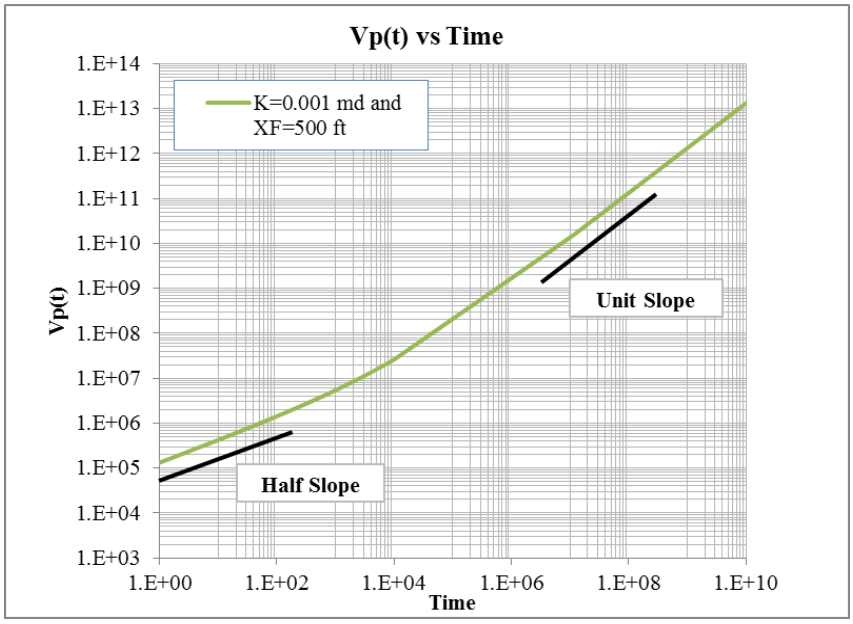

Figure 8 Drainage volume type curve

If the permeability is increased, drainage volume curve shifts to the left, refer Fig. 9. If the fracture length is changed, curve shifts in the upward direction with increase in length, in the region where flow is linear in nature, but for the later time it converges to the same as for long time fracture of different length acts radially, refer Fig. 10.

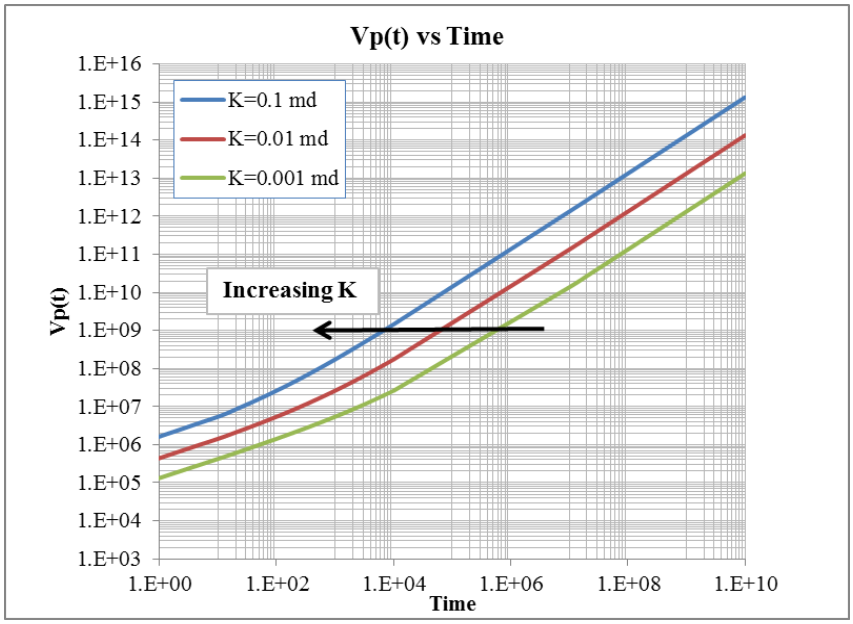

Figure 9 Drainage volume plot with variation in permeability

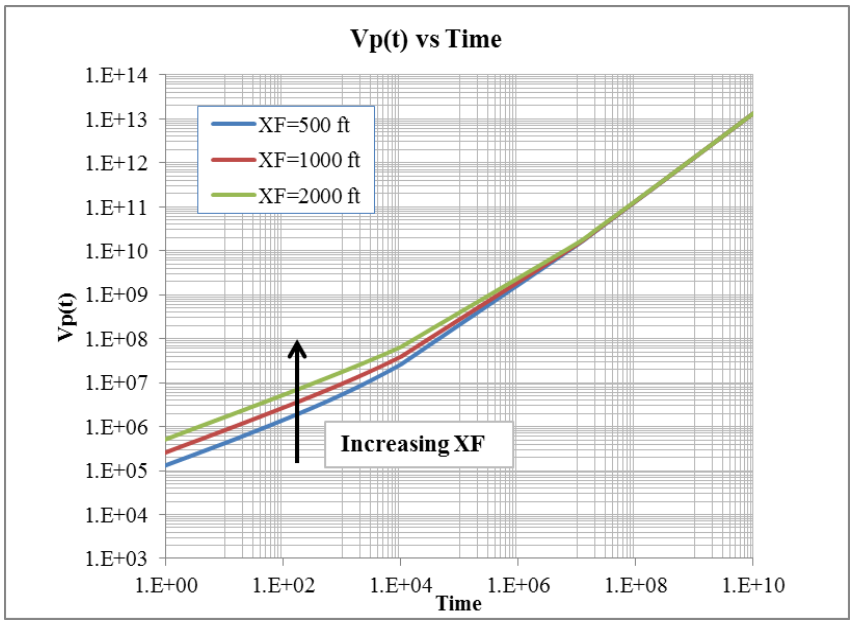

Figure 10 Drainage volume plot with variation in fracture length

3.1.2 Approximate elliptical model

The assumption for this case is the same as the earlier derivation. The fracture is considered to be fully completed throughout the formation and is of infinite conductivity. Reservoir is homogeneous in nature.

Here the diffusivity is the same throughout as the reservoir is homogeneous in nature. For the drainage volume geometry we are considering an elliptical shape as shown in the analytical solution for diffusivity equation [3, 19, 22]. The two focal points for the ellipse are the end points of the fracture and the major and minor axis are shown in Fig. 11. Here it is assumed that the pressure wave has moved to the same radial distance of r from the end points as well as from the center of the fracture. Following Fig. 11 shows the shape of the pressure wave propagation.

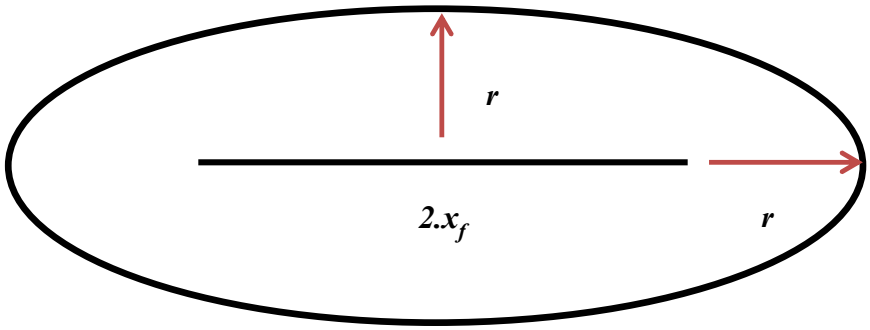

Figure 11 Approximate ellipse as pressure front

It is assumed that the fracture is of the infinite conductivity so throughout the fracture our DTOF is zero. Drainage volume in elliptical shape is actually a combination of the radial and the linear flow. For the initial time the ellipse converges to a very thin line i.e. the fracture and the flow is linear formation in nature. For the later stage it is radial in nature.

Now following the same sequence for the derivation as earlier.

We have, for homogeneous media, $\delta\tau = \sqrt{\frac{\phi\mu c_t}{k}} \cdot \delta r$ or $\tau = \sqrt{\frac{\phi\mu c_t}{k}} \cdot r$ or $\sqrt{\alpha} \cdot \tau = r$

Now, for this geometry,

Major axis: $r + x_f$

Minor axis: r

Drainage Volume (geometrically),

$$V_p(r) = \pi.r.(r + x_f).h.\phi = (\pi.r^2 + \pi.r.x_f).h.\phi \tag{33}$$

Now substituting $\sqrt{\alpha} \cdot \tau = r$,

$$V_p(\tau) = (\pi\alpha\tau^2 + \pi x_f \sqrt{\alpha}\tau).h.\phi$$

$$w(\tau) = \frac{dV_p(\tau)}{d\tau} = (2\pi\tau\alpha + \pi.x_f \sqrt{\alpha}).h.\phi \tag{34}$$

$$V_p(t) = \int_0^\infty \frac{dV_p(\tau)}{d\tau}.e^{-\frac{\tau^2}{4t}} = \int_0^\infty w(\tau).e^{-\frac{\tau^2}{4t}} d\tau$$

$$V_p(t) = \int_0^\infty (2\pi\tau\alpha + \pi.x_f \sqrt{\alpha}).h.\phi.e^{\frac{-\tau^2}{4t}}.d\tau = h.\phi.(4\pi.\alpha.t + \pi.x_f \sqrt{\pi.\alpha.t}) \tag{35}$$

$$V_p(t) = h.\phi.(\frac{4\pi}{\phi\mu c_t}.[k].t + \pi.\sqrt{\frac{\pi}{\phi\mu c_t}}.(x_f.\sqrt{k}).\sqrt{t}) \tag{36}$$

Similar to pill box case this case also has the drainage volume equation which has one part linear to the time and the other part to the square root of time. For the small time the coefficient of square root of time is more significant and for the large time the coefficient of linear time is more significant. This results only differs from the pill box in terms of the effective fracture area. For earlier case it is

On the log-log plot we have the drainage volume which has half slope for small time and for large time we have unit slope. Here, for this case we get the information for $h.\frac{4\pi}{\mu c_t}.k$ from the unit slope part and $\pi.h.\sqrt{\frac{\pi\phi}{\mu c_t}}.(x_f.\sqrt{k})$ from the half slope part.

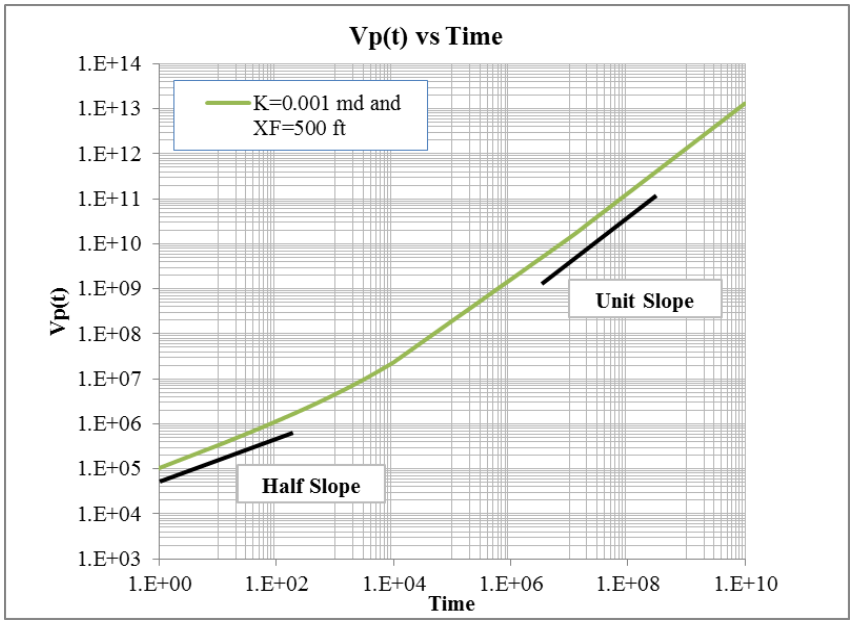

Figure 12 Drainage volume plot

Following are the plots for the variation in the Permeability and Fracture length.

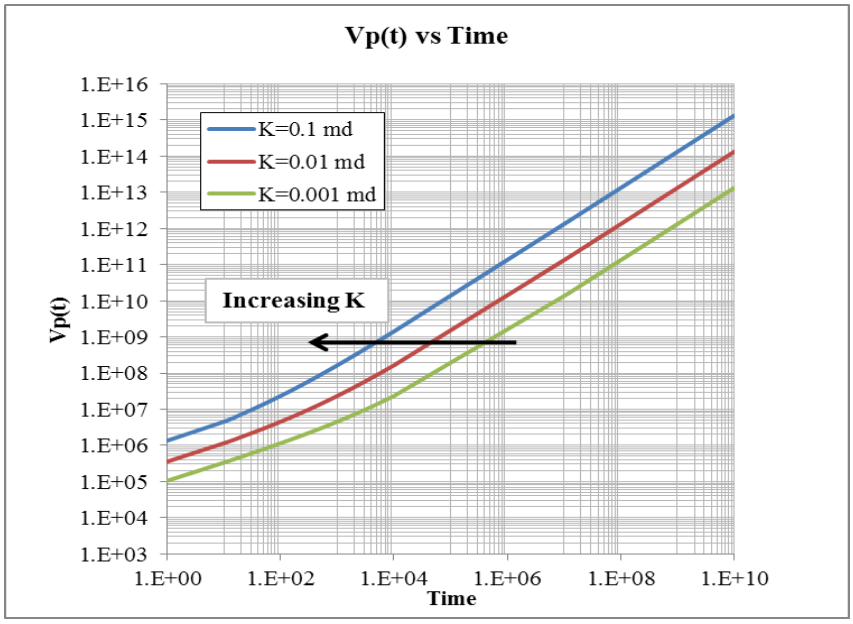

Figure 13 Drainage volume plot with variation in permeability

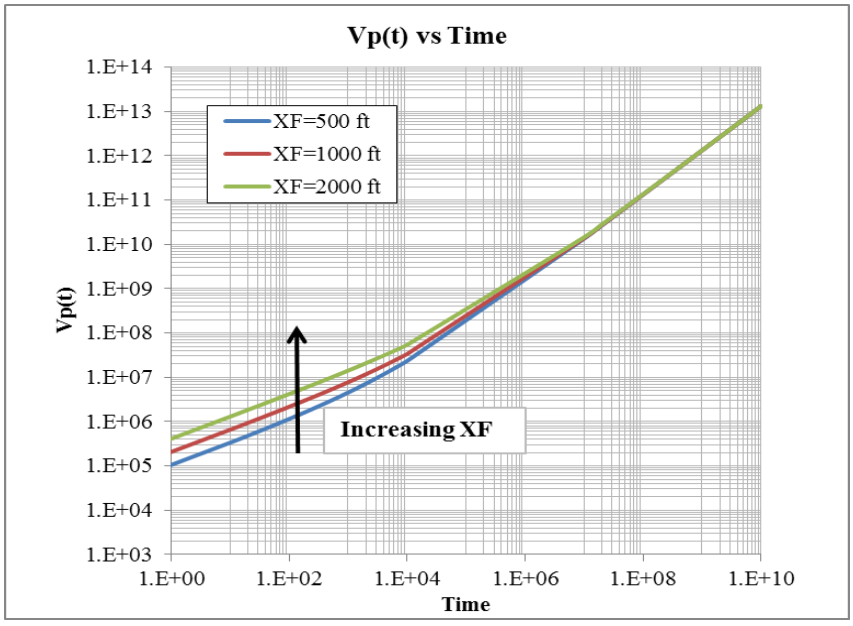

Figure 14 Drainage volume plot with variation in fracture length

3.1.3 Exact ellipse

Here for this case we have assumed perfect elliptical pressure wave propagation. For this derivation we have started from the basic diffusivity equation. Like in the earlier literature starting point is the diffusivity equation and later we combine our methodology with it to get the relationship for the drainage volume.

Now the starting point is the Diffusivity Equation,

Diffusivity Equation:

$$\nabla^2 p = \frac{\phi \mu c_t}{k} \frac{\partial p}{\partial t} \tag{37}$$

For Cartesian Co-ordinate System:

$$\frac{\partial^2 p}{\partial x^2} + \frac{\partial^2 p}{\partial y^2} = \frac{\phi \mu c_t}{k} \frac{\partial p}{\partial t} \tag{38}$$

Elliptical Coordinates Transformation

$$\begin{aligned} \text{x} &= \text{L}.\ \cosh\xi.\ \cos\eta \\ \text{y} &= \text{L}.\ \sinh\xi.\ \sin\ \eta \end{aligned} \tag{39}$$

Here L is the fracture half length.

Now, writing the Eikonal Equation in Elliptical Coordinate System.

$$\frac{\phi \mu c_t}{k} = \left|\nabla \tau\right|^2 = \left(\nabla \xi \frac{\partial \tau}{\partial \xi} + \nabla \eta \frac{\partial \tau}{\partial \eta} \right) . \left(\nabla \xi \frac{\partial \tau}{\partial \xi} + \nabla \eta \frac{\partial \tau}{\partial \eta} \right) \tag{40}$$

$$\left|\nabla\xi\right|^2 = \left|\nabla\eta\right|^2 = \frac{1}{L^2.(\sinh^2\xi + \sin^2\eta)} \tag{41}$$

and

$$\nabla\xi.\nabla\eta = 0 \tag{42}$$

Hence,

$$\frac{\phi\mu c_t}{k} = \left|\nabla\tau\right|^2 = \frac{1}{L^2.(\sinh^2\xi + \sin^2\eta)}\left(\left(\frac{\partial\tau}{\partial\xi}\right)^2 + \left(\frac{\partial\tau}{\partial\eta}\right)^2\right) \tag{43}$$

Since ours terms in η are negligible as compared to the other terms in the equation i.e $sin^2\eta \ll sinh^2\xi$, so we can make an assumption that $\frac{\partial\tau}{\partial\eta} = 0$.

Now,

$$\frac{\partial\tau}{\partial\xi} = \sqrt{\frac{\phi\mu c_t}{k}}.L.\sqrt{(\sinh^2\xi + \sin^2\eta)} \tag{44}$$

We can neglect $\sin^2\eta$ with respect to $\sinh^2\xi$ or take an average value for the function because when value of ξ increases hyperbolic function will become bigger than the trigonometric function.

The average value for the $\sin^2\eta$ is $\frac{1}{2}$. Now the Diffusive Time of Flight is related to the elliptical coordinates in the following formula.

$$\frac{\partial \tau}{\partial \xi} = \sqrt{\frac{\phi \mu c_t}{k}}.L.\sqrt{\sinh^2 \xi + \frac{1}{2}} = \sqrt{\frac{\phi \mu c_t}{k}}.\frac{L}{\sqrt{2}}.\sqrt{\cosh 2\xi} \tag{45}$$

This could be simplified and integrated. The solution to the integral is in the form of the Hypergeometric function[27].

$$\tau = \sqrt{\frac{\phi \mu c_t}{k}}.\frac{L}{2}.\left(-e^{-\xi}\sqrt{e^{4\xi}+1} + 2.\left(e^{3\xi}.\ \text{Hypergeometric}\left(\frac{1}{2},\frac{3}{4};\frac{7}{4},e^{-4\xi}\right) - \frac{1}{3}.\ \text{Hypergeometric}\left(\frac{1}{2},\frac{3}{4};\frac{7}{4},-1\right)\right)\right)$$

Now the Drainage Volume for an elliptical geometry may be obtained.

$$V_p(\xi) = \frac{1}{2}.\pi.L^2.h.\phi.\sinh(2\xi) \tag{46}$$

$$V_p(t) = \int_0^{\infty}\left(\frac{dV_p}{d\xi}.\frac{d\xi}{d\tau}\right).e^{\frac{-\tau^2}{4t}}.d\tau \tag{47}$$

Eq.(47) can be integrated numerically and the expression within the integration can be evaluated based on the relationship by Eq.(46),(47).

This solution is numerically very extensive in nature. In addition to this, a better solution is discussed next.

This is another way of formulation for elliptical drainage volume geometry. Here the pressure wave is assumed to be propagating as an ellipse. A minor modification in the derivation is made as compared to the earlier derivation where we used the basic solution of diffusivity equation in elliptical coordinate system. In the following Fig. 15 the pressure wave is at the distance r from the fracture.

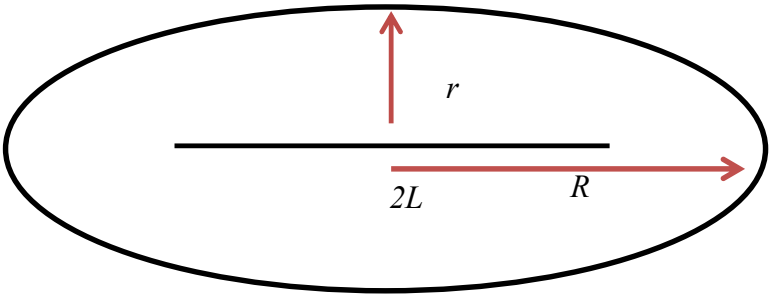

Figure 15 Pressure wave front geometry

Elliptical Coordinates Transformation

$$x = L.\cosh\xi.\cos\eta$$
$$y = L.\sinh\xi.\sin\eta$$

When $\eta = 90°$ we have, $r = L.\sinh\xi$, which is the minor axis of the ellipse.

When $\eta = 0°$ we have, $R = L.\cosh\xi$, which is the major axis of the ellipse.

Now, R could be written in terms of the r,

$$R = L.\sqrt{\frac{L^2 + r^2}{L^2}} = \sqrt{L^2 + r^2}$$

Now, $V_p(r) = h.\phi.\pi.r.R = h.\phi.\pi.r\sqrt{L^2 + r^2}$

We have from the earlier derivation for the elliptical system,

$$\frac{\phi\mu c_t}{k} = |\nabla\tau|^2 = \frac{1}{L^2.(\cosh^2\xi - \cos^2\eta)}\left(\left(\frac{\partial\tau}{\partial\xi}\right)^2 + \left(\frac{\partial\tau}{\partial\eta}\right)^2\right)$$

Since ours terms in η are negligible as compared to the other terms in the equation i.e $cos^2\eta \ll cosh^2\xi$, so we can make an assumption that $\frac{\partial\tau}{\partial\eta} = 0$..

Now we have, $\frac{\partial\tau}{\partial\xi} = \sqrt{\frac{\phi\mu c_t}{k}}.L.\sqrt{\cosh^2\xi - \cos^2\eta}$. Again, since $\cosh^2\xi >> \cos^2\eta$:

$$\frac{\partial\tau}{\partial\xi} = \sqrt{\frac{\phi\mu c_t}{k}}.L.\cosh\xi \tag{48}$$

By integration, $\tau = \sqrt{\frac{\phi\mu c_t}{k}}.L.\sinh\xi$ or $\tau = \sqrt{\frac{\phi\mu c_t}{k}}.r$ or $r = \sqrt{\alpha}.\tau$ where $\alpha = \frac{k}{\phi\mu c_t}$

$$\frac{\partial \mathrm{V_p}(r)}{\partial r} = \frac{\partial(\mathrm{h}.\phi.\pi.\mathrm{r}\sqrt{\mathrm{L}^2 + r^2})}{\partial r} = \mathrm{h}.\phi.\pi.\left(\frac{\mathrm{L}^2 + 2r^2}{\sqrt{\mathrm{L}^2 + r^2}}\right)$$

$$w(\tau) = \frac{\partial \mathrm{V_p}(\tau)}{\partial\tau} = \frac{\partial \mathrm{V_p}(r)}{\partial r}\frac{\partial \mathrm{r}}{\partial\tau} = \mathrm{h}.\phi.\pi.\left(\frac{\mathrm{L}^2 + 2\alpha\tau^2}{\sqrt{\mathrm{L}^2 + \alpha\tau^2}}\right).\sqrt{\alpha} \tag{49}$$

We know that,

$$V_p(t) = \int_0^\infty \frac{dV_p(\tau)}{d\tau}.e^{-\frac{\tau^2}{4t}} = \int_0^\infty w(\tau).e^{-\frac{\tau^2}{4t}}d\tau$$

$$V_p(t) = \int_0^\infty \mathrm{h}.\phi.\pi.\left(\frac{\mathrm{L}^2 + 2\alpha\tau^2}{\sqrt{\mathrm{L}^2 + \alpha\tau^2}}\right).\sqrt{\alpha}.e^{-\frac{\tau^2}{4t}}d\tau$$

On integration [27],

$$V_p(t) = \frac{\pi.h.\phi.L^2}{2}.e^{\frac{L^2}{8\alpha t}}.BesselK[1,\frac{L^2}{8\alpha t}] \quad (50)$$

Where $\alpha = \frac{k}{\phi\mu c_t}$

Plot of the above Drainage Volume is as follows:

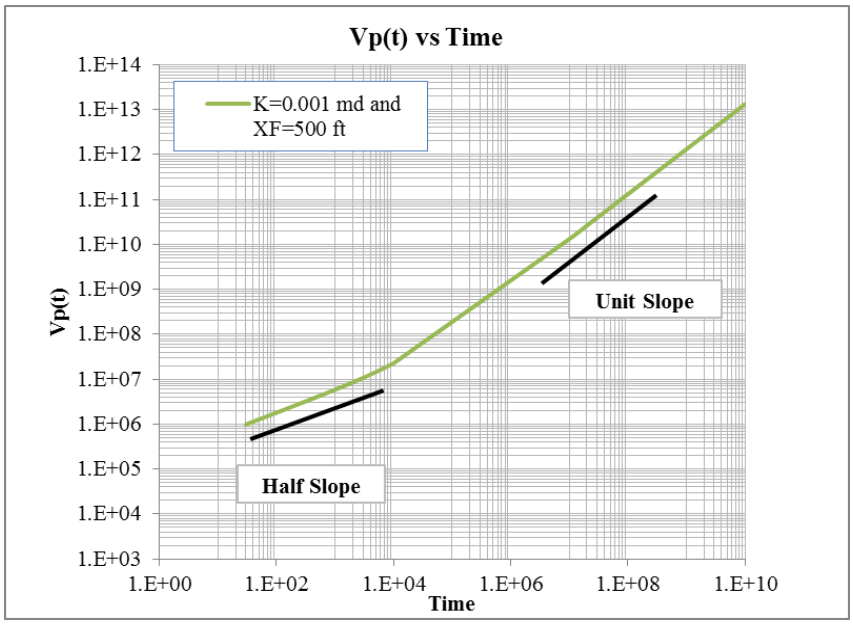

Figure 16 Drainage volume plot

Drainage Volume plots for the variation in the permeability and fracture length are shown below.

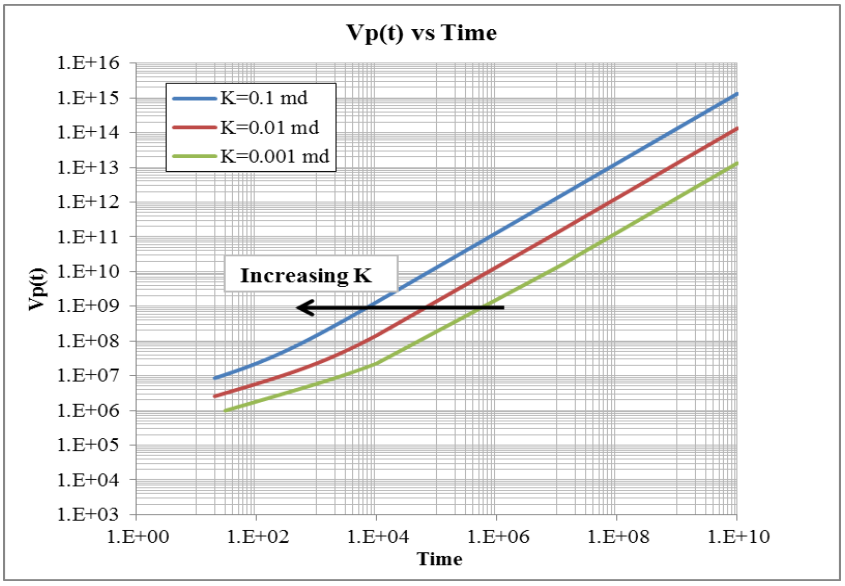

Figure 17 Drainage volume plot with variation in permeability

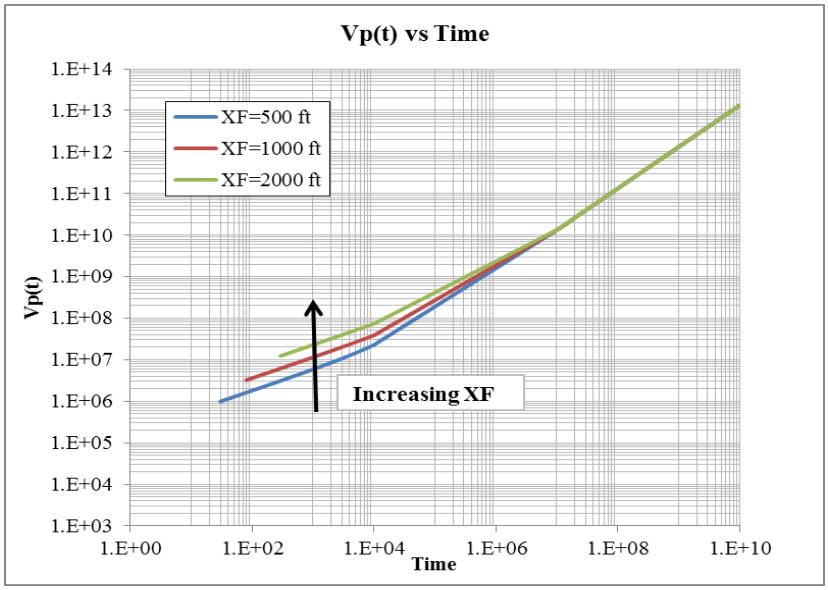

Figure 18 Drainage volume plot with variation in fracture length

3.1.4 Comparison of the analytical models

Following are the plots for drainage volume of three models combined together.

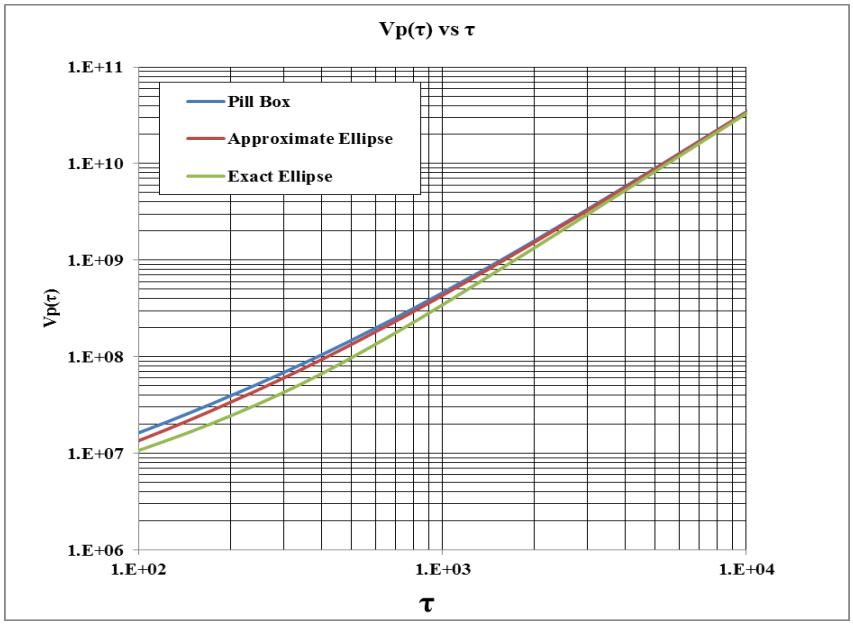

Figure 19 Drainage volume vs tau (DTOF)

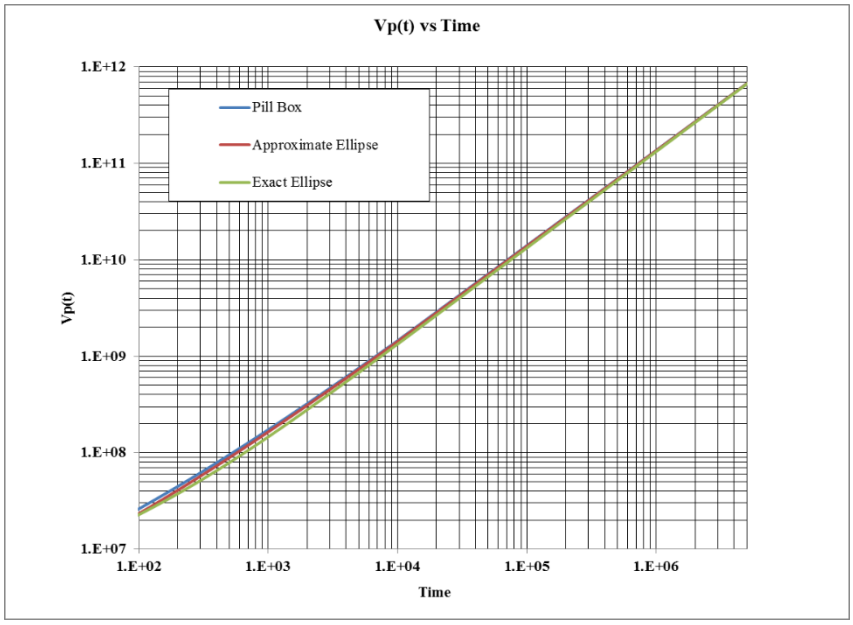

Figure 20 Drainage volume vs time

From Fig. 19, we can say that the drainage volume for the pill box shape is more as compared to that of the elliptical shapes for small τ values. There may be a possibility that drainage volume from the pill box shape is an overestimate of actual situation. Moreover when transition from the linear to radial is taking place, i.e. when the slope is changing, we see that approximate ellipse is higher than the estimate of the exact elliptical solution. That leads to the conclusion that the assumption of the same growth in the minor and major axis of the ellipse for approximate ellipse solution may not be correct.

Now in Fig. 20, which is the estimate of the drainage volume as function of time, we see the same nature of the difference in estimates of the drainage volume as we have seen in Fig. 19. That is due to the fact that the integration which is evaluated over a function ($w(\tau)$) which itself is more.

Now the question arises which of the three models is correct and more applicable? Answer to this question is explored by a synthetic case and welltest derivative theory.

3.1.4.1 Comparison based on simulation study

A simple model of fully completed single infinite conductivity fracture is taken for the analysis. Water is used as fluid for running the flow simulation. Production was simulated for 16,916 days. Parameters for simulation are shown in the following table.

Table 1 Parameter for single infinite conductivity fracture

Parameter	Value
Reservoir size	2005×2005×205 ft^3
Initial pressure	5000 psi
Flow rate	0.5 stb/day
Matrix porosity	0.01
Matrix permeability	0.0001 mD
Hydraulic fracture porosity	0.001
Hydraulic fracture permeability	10000 mD
Hydraulic fracture width	0.2 ft
Hydraulic fracture half-length	252.5 ft

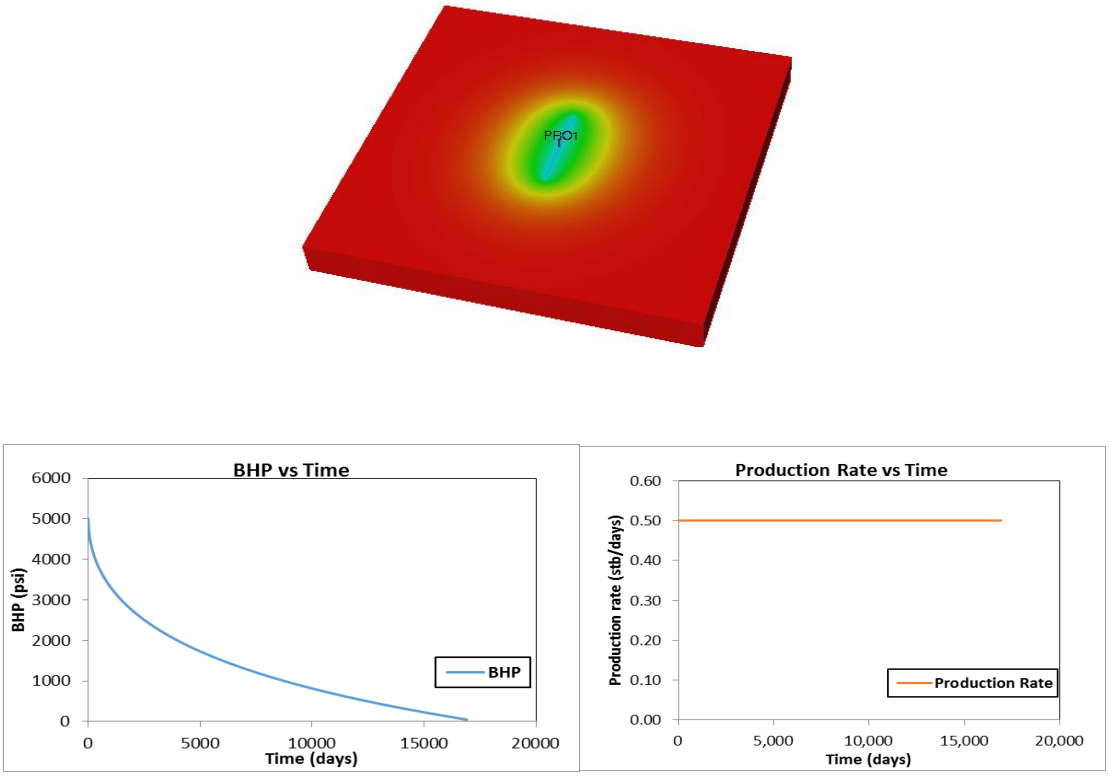

Figure 21 Simulation data for single infinite conductivity fracture

Based on the simulation data, drainage volume was calculated. Drainage volume from the fixed parameters of simulation were used for plotting drainage volume for the three models. All plots are shown together below.

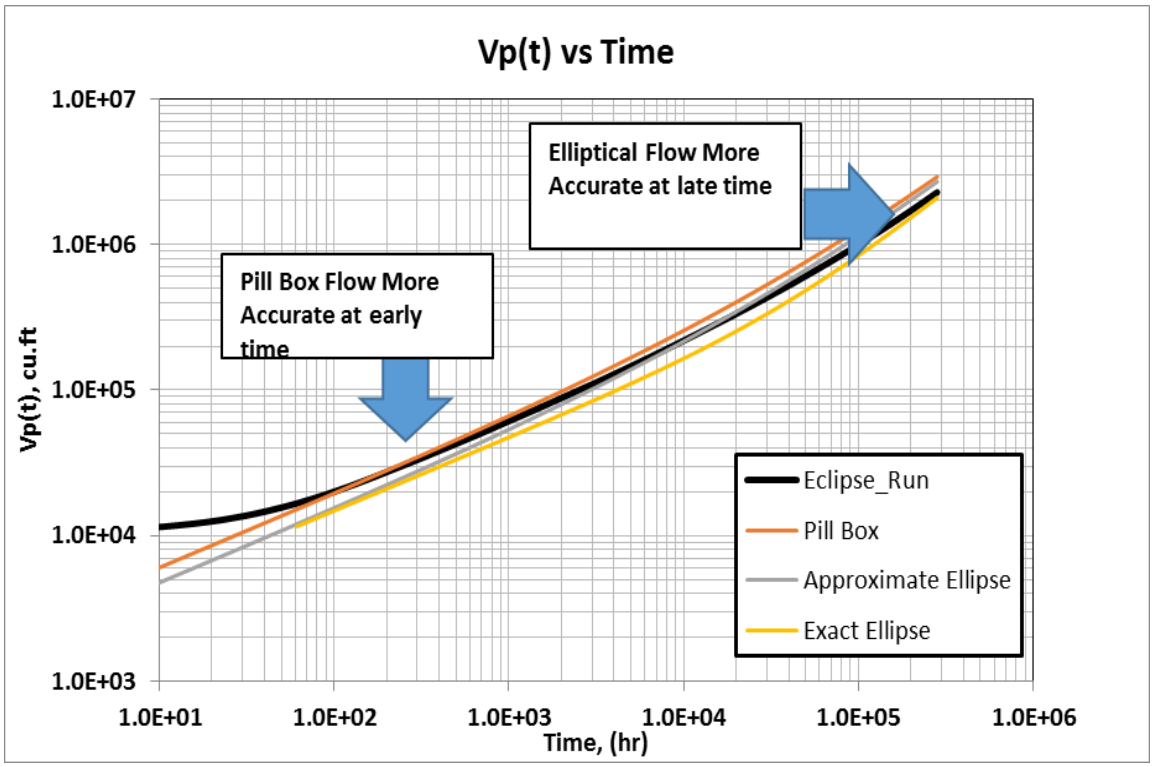

Figure 22 Drainage volume for simulation data and three models

As shown in the Fig. 22 for early time, the pill box model is more accurate as it matches with the plot of the simulation case. For later time, the drainage volume is more consistent with the exact ellipse model. It can be hence inferred that the pill box model is more consistent for the formation linear case as we know the pressure propagation is more in the lateral direction as compared to the elliptical case. For the later time pressure wave more turned into the elliptical shape which is the reason for the matching of the model for the

later time. Late time performance is consistent with the definition of well productivity for flow around an infinite conductivity fracture.

3.1.4.2 Comparison based on the welltest derivative

Welltest derivative is used in the pressure transient analysis for a fractured well. Welltest derivative plots are used for the identification of the flow regime for transient data. Here we have compared our models based on the welltest derivative theory.

Welltest derivative plots and the limits for the different flow are explained in the available literature. Welltest derivative is a log-log plot of $t_{L_fD}\frac{\partial p_D}{\partial t_{L_fD}}$ versus t_{L_fD}, where

$t_{L_fD}=\frac{0.0002637kt}{\phi\mu c_t L_f^2}$ and $P_D=\frac{kh\left(P_i-P_{wf}\right)}{141.2qB\mu}$.

For the linear flow regime (early time) $t_{L_fD}\frac{\partial p_D}{\partial t_{L_fD}}=\frac{1}{2}\left(\pi t_{L_fD}\right)^{\frac{1}{2}}$ when $t_{L_fD}\le 0.016$.

For pseudo radial flow (for long time) $t_{L_fD}\frac{\partial p_D}{\partial t_{L_fD}}$ is constant when $t_{L_fD}\ge 3$ [28].

According to our methodology, for a fixed rate draw-down in an infinite domain

$$c_t\frac{\partial p}{\partial t}=\frac{1}{w(\tau)}\frac{\partial q}{\partial \tau}=-\frac{q_w}{V_p(t)}e^{-\tau^2/4t}$$

For well location,$\tau=0$, thus $c_t\frac{\partial p}{\partial t}=-\frac{q_w}{V_p(t)}$

On combining the welltest derivative equations and our methodology of the drainage volume we have

$$t_{L_f D}\frac{\partial p_D}{\partial t_{L_f D}} = \frac{kh}{141.2B\mu}\times\frac{t}{c_t V_p(t)} \tag{51}$$

For comparison we have assumed fixed parameters and compared the three models together. The parameters which were used are in the below table.

Table 2 Parameters for generating curves

Parameter	Value
Porosity	0.01
Viscosity (cp)	1
Permeability (md)	0.0001
Compressibility (psi^{-1})	1.00E-05
Fracture Half Length (ft)	500
Height (ft)	200

Welltest derivative plot based on above parameters is plotted below.

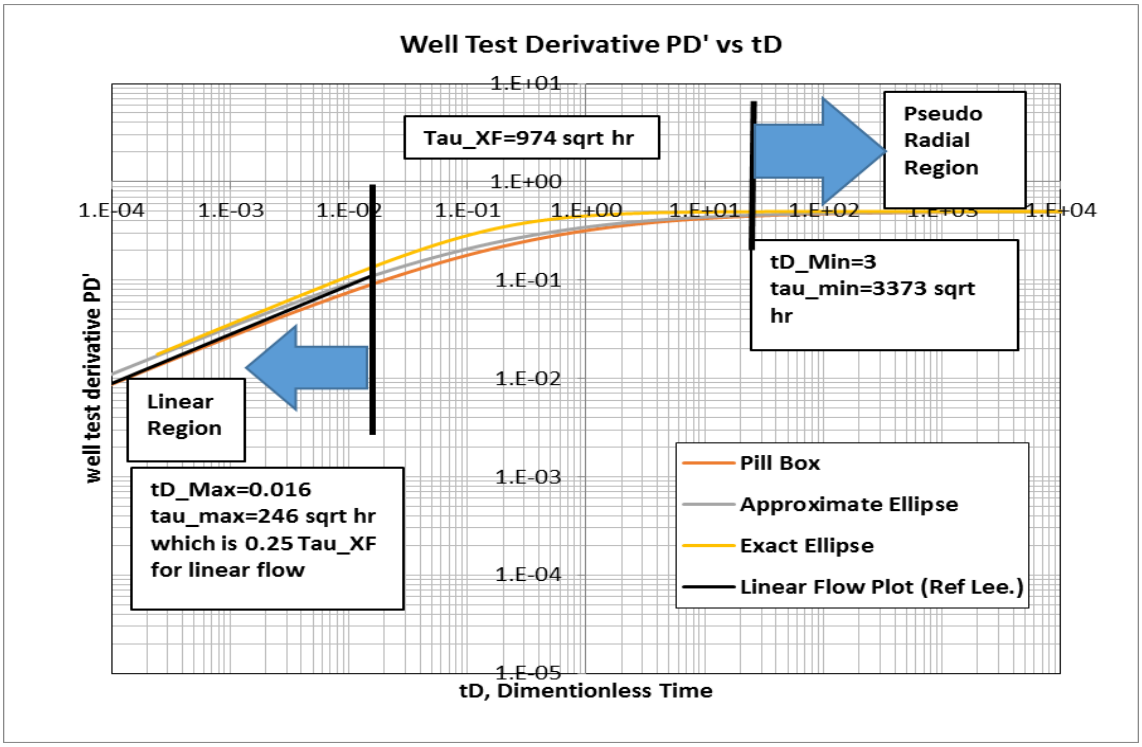

Figure 23 Welltest derivative plots for the different models

From this plot we can infer that for lower τ values our pill box model is more accurate ($\tau < 0.25\ \tau_{X_f}$). For early time the pill box model for the drainage volume is applicable.

For the higher τ values ($\tau > 3.5\ \tau_{X_f}$), when pseudo radial flow takes place, all models converge to the same results. Thus for later time all models start behaving identically when comparing flow behaviors.

Application of the pill box model is justified when we use it for a case where we do not reach very high τ values.

3.1.5 Observation and recommendation

Three models were used for the derivation of the analytical solution of drainage volume for infinite conductivity fractured well. Our assumption for defining the drainage volume geometry was justified for derivations. The most accurate model out of the three models cannot be judged without considering its application.

The pill box model is most accurate when the pressure wave is near the fracture, while all models converge to the same results for larger values. In the two comparison studies it is clear that the pill box model is most applicable for the earlier time frames than the other model.

Question is do we really reach to a point of larger values in τ when actually producing from the low permeability regions? For shale gas we do not reach to such extent. Moreover for horizontal well with multiple fractures generally the fracture spacing is maintained below half of the fracture half length. Thus for the application to practical cases use of the pill box Model is more justified and applicable.

4. NEW APPROACH FOR PRODUCTION ANALYSIS

There are multiple analytical techniques for the analysis of the production data. These techniques, however, are model based and can be mostly applied in conventional scenarios. These analytical techniques are limited to homogeneous cases. Here a new technique has been developed which works directly on the field data, i.e. production and pressure data.

In Fig. 24 we can see that when the propagation of fracture takes place it is not sure that it will follow particular model. Due to this we need a model free analysis technique.

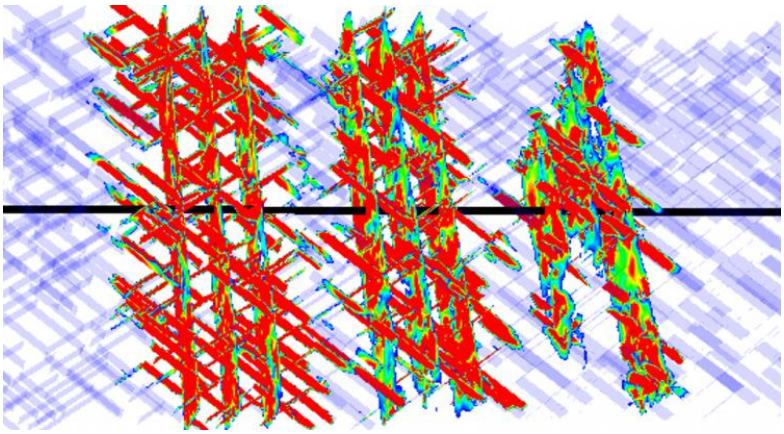

Figure 24 Hydraulic fracture propagation with natural fractures [29]

This approach for the analysis is based on the drainage volume. A new variable of the Instantaneous Recovery Ratio (I.R.R) which is the ratio of total produced volume to the drainage volume is defined. In addition, $w(\tau)$ function is calculated. The $w(\tau)$ function is related to the area of fracture and reservoir properties.

In order to determine drainage volume from the production data, this approach uses the Rate Normalized Pressure (RNP) and pressure transient concepts.

4.1 New method for production data analysis

New method for the production data analysis consists of determination of three plots:

1. Drainage Volume vs Time
2. Instantaneous Recovery Ratio (IRR)
3. $w(\tau)$ vs τ

All these plots can be directly estimated from the production data for the well. In the next section it will be explained how these plots can be estimated from the production data theoretically.

4.1.1 Drainage volume from production data

The exposition presented in this section closely follows what was presented in Yang, C., et al (2015).

Asymptotic solution to the diffusivity equation is shown in the literature review. For fixed rate drawdown and infinite domain we have:

$$c_t \frac{\partial p}{\partial t} = \frac{1}{w(\tau)} \frac{\partial q}{\partial \tau} = -\frac{q_w}{V_p(t)} e^{-\tau^2/4t} \tag{52}$$

Above equation is the starting point for our method for analysis. From this equation we can directly get the drainage volume estimates. However this equation can only be applied for a fixed flow rate.

For slowly varying flow rate, we can use instantaneous flow rate $q_w(t)$ despite the fixed flow rate. For our usage we have modified Eq.52 as:

$$c_t \frac{\partial p}{\partial t} = \frac{1}{w(\tau)} \frac{\partial q}{\partial \tau} = -\frac{q_w(t)}{V_p(t)} e^{-\tau^2/4t} \tag{53}$$

When dealing with the pressure transient analysis, we can link the welltest derivative with the drainage volume with help of the following equation:

$$\Delta p'_{wf} = \frac{d\Delta p_{wf}}{d \ln t} = \frac{q_w t}{c_t V_p(t)} e^{-\tau_w^2/4t} \approx \frac{q_w t}{c_t V_p(t)} \tag{54}$$

If we have the well production data with the variable flow and pressure data, we can calculate the drainage volume by the following equation,

$$\frac{d\Delta p_{wf}(t)}{dt} = \frac{q_w(t)}{c_t V_p(t)} e^{-\tau_w^2/4t} \approx \frac{q_w(t)}{c_t V_p(t)} \tag{55}$$

As per the earlier work for unconventional reservoir, the use of rate normalized pressure is recommended. Here the rate normalized pressure concept is being used but in a modified form. We considered calculation of derivative in terms of the cumulative volume produced rather than working in terms of time.

$$W_p(t) = \int_{t=0}^{t} q_w(t) dt \tag{56}$$

$$dW_p(t) = q_w(t) dt \tag{57}$$

Now,

$$\frac{d\Delta p_{wf}(t)}{dt} \approx \frac{q_w(t)}{c_t.V_p(t)} \Rightarrow \frac{c_t}{q_w(t)} \frac{d\Delta p_{wf}(t)}{dt} \approx \frac{1}{V_p(t)} \tag{58}$$

Therefore, $$\frac{1}{V_p(t)} \approx c_t \frac{d\Delta p_{wf}(t)}{dW_p(t)} \tag{59}$$

4.1.2 Instantaneous Recovery Ratio (IRR) from the production data

Instantaneous Recovery Ratio (IRR) is the ratio of hydrocarbon produced at any time to the drainage volume at that time. IRR shows instantaneous recovery, it is not to be confused with the ultimate recovery of the reservoir. IRR gives an indication of how fast the production is as compared to the increase in drainage volume. The IRR plots for the production data shows a change whenever there is change in the rate of change of drainage volume expansion i.e. when a flow regime changes.

Whenever a fracture job is done, it creates a fracture area or area for flow of the hydrocarbon to the fracture from the rock. This creates a pressure wave propagation which is the basis of our methodology. The pressure wave propagates and creates drainage volume. It is always possible that the pressure wave increases faster as compared to the production being taken out. This IRR estimate gives a comparative view when plotted for different wells together.

From the production data, IRR can be directly calculated like the drainage volume calculations.

$$IRR(t) = \frac{W_p(t)}{V_p(t)} \approx c_t \frac{d\Delta p_{wf}(t)}{d \ln W_p(t)} \tag{60}$$

4.1.3 $w(\tau)$ from the production data

From the production data, as specified earlier, we can get the drainage volume. Now this drainage volume data can be used for the $w(\tau)$ estimation.

$w(\tau)$ is an important function as it relates to the spatial distribution of the drainage volume. It is indirectly related to the surface area of the drainage volume in the spatial coordinate τ, DTOF. $w(\tau)$ function is defined as the derivative of the drainage volume in spatial coordinate i.e. $w(\tau) = \frac{dV_p(\tau)}{d\tau}$.

The main equation which relates the drainage volume, $V_p(t)$ to the $w(\tau)$ function is $V_p(t) = \int_0^\infty w(\tau) e^{-\tau^2/4t} d\tau$. This equation is inverted to get the estimates of $w(\tau)$. Two techniques can be used for the inversion.

4.1.3.1 $w(\tau)$ inversion by piecewise constant representation

Here, $w(\tau)$ function is assumed to be piecewise constant. The integral which relates $w(\tau)$ to $V_p(t)$ is approximated by a finite integral with small intervals within which a constant value of $w(\tau)$ is assumed. This piecewise constant value is then estimated.

Our basic main equation is

$$V_p(t) = \int_0^{\infty} w(\tau) e^{-\tau^2/4t} d\tau$$

This equation is divided into finite intervals as:

$$V_p(t_i) = \sum_{j=1}^{N} \int_{\tau_{ja}}^{\tau_{jb}} w_j(\tau) \exp\left(-\frac{\tau^2}{4t_i}\right) d\tau \tag{61}$$

Here intervals of $\tau_{ja}$to τ_{jb} where $w_j(\tau)$ is considered as piecewise constant are used. This is a good assumption if a sufficient number of intervals are taken. This equation can be written in terms of the error function for each interval.

$$V_p(t_i) = \sqrt{\pi t_i} \sum_{j=1}^{N} w(\tau_j) \cdot \left(Erf\left(\frac{\tau_{jb}}{2\sqrt{t_i}}\right) - Erf\left(\frac{\tau_{ja}}{2\sqrt{t_i}}\right)\right) \tag{62}$$

This can be established as a combination of linear equations. It can be expressed as a linear matrix equation A*x*=b

where, $a_{ij} = \sqrt{\pi t_i}\left(Erf\left(\frac{\tau_{jb}}{2\sqrt{t_i}}\right) - Erf\left(\frac{\tau_{ja}}{2\sqrt{t_i}}\right)\right)$, $x_i = w(\tau_i)$ and $b_i = V_p(t_i)$

This equation could not be solved directly as matrix A turns out to be singular. The reason is that the error function reaches close to unity once argument value is near to 2.5. Once the coefficient matrix becomes singular it is hard to solve this system of equation. It could be said very clearly that beyond this value, coefficient will reduce to zero or very small values and does not contribute to the results. Upper limit can be set for anytime t to be 5√t.

For the first step or the smallest time value we can direct calculate the value of (τ_1) . Now for any nth value, n-1 values of $w(\tau)$ have already been solved and these values can be used to calculate the nth value in the interval $\left[2\sqrt{t_{i-1}}, 2\sqrt{t_i}\right]$.

$$V_p(t_1) = \sqrt{\pi t_1}\, w(\tau_1) \cdot \left(Erf\left(\frac{5\sqrt{t_1}}{2\sqrt{t_1}}\right) - Erf\left(\frac{0}{2\sqrt{t_1}}\right)\right) \approx \sqrt{\pi t_1}\, w(\tau_1)$$

$$V_p(t_2) = \sqrt{\pi t_2}\, w(\tau_1) \cdot \left(Erf\left(\frac{2\sqrt{t_1}}{2\sqrt{t_2}}\right) - Erf\left(\frac{0}{2\sqrt{t_2}}\right)\right) + \sqrt{\pi t_2}\, w(\tau_2) \cdot \left(Erf\left(\frac{5\sqrt{t_2}}{2\sqrt{t_2}}\right) - Erf\left(\frac{2\sqrt{t_1}}{2\sqrt{t_2}}\right)\right)$$

$$V_p(t_n) = \sqrt{\pi t_n} \sum_{j=1}^{n-1} w(\tau_j) \cdot \left(Erf\left(\frac{2\sqrt{t_j}}{2\sqrt{t_n}}\right) - Erf\left(\frac{2\sqrt{t_{j-1}}}{2\sqrt{t_n}}\right)\right) + \sqrt{\pi t_n}\, w(\tau_n) \cdot \left(Erf\left(\frac{5\sqrt{t_n}}{2\sqrt{t_n}}\right) - Erf\left(\frac{2\sqrt{t_{n-1}}}{2\sqrt{t_n}}\right)\right)$$

From this we can get the estimate of $w(\tau)$ for the different τ intervals.

For testing, data for one well is inverted and shown below:

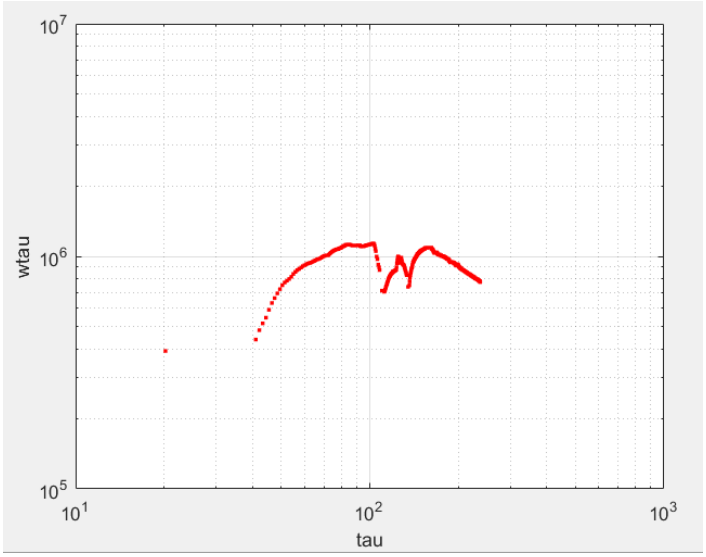

Figure 25 w(τ) inversion by a piecewise constant representation

4.1.3.2 $w(\tau)$ inversion by Stehfest

Here, we are trying to express our function in the form of Laplace transform. Our starting point equation is

$$V_p(t) = \int_0^\infty w(\tau) e^{-\tau^2/4t} d\tau$$

So we can say, $d\tau = \frac{d\tau^2}{2\tau}$

Now,

$$V_p(t) = \int_0^\infty \frac{w(\tau)}{2\tau} e^{-\tau^2/4t} d\tau^2$$

Now if we say $\tau^2 = u, \frac{w(\tau)}{2\tau} = f(u)$ and $\frac{1}{4t} = s, V_p(t) = F(s)$

$$F(s) = \int_0^\infty f(u) e^{-s.u} du \tag{63}$$

Here, Laplace space is $\frac{1}{4t} = s$ and original space is $\tau^2 = u$

From field data we have numerical value of $V_p(t)$ vs t, i.e. F(s) vs s. Now we can use Stehfest technique for the numerical inversion.

Stehfest is a well-known method for numerical inversion of the Laplace. But this method works only if we know the analytical form of the function in Laplace space. Here we know

the values and they are based on the production data. So there is a high probability that there will be multiple problems in the accuracy of the estimates.

For testing, data for one well is inverted and shown below:

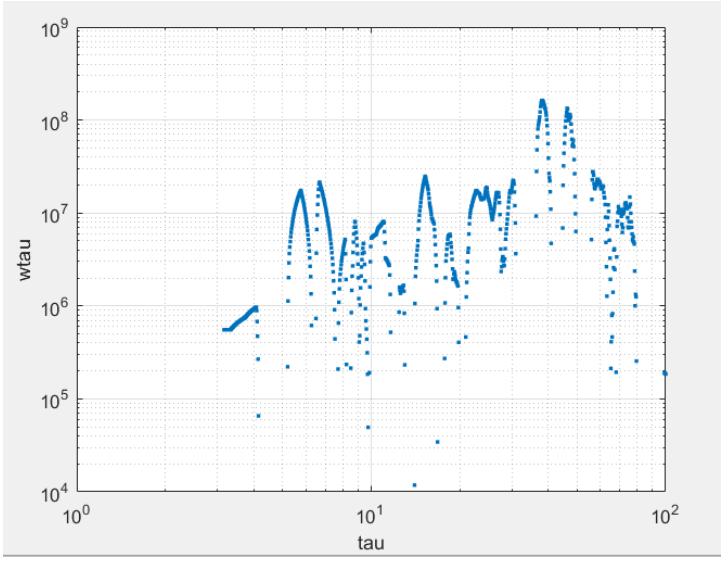

Figure 26 w(τ) Inversion by Stehfest

Our inversion from the Stehfest techniques is not very accurate as it show instability throughout the plot. For field applications we will follow the piecewise inversion technique.

4.2 Application of method for production analysis

Approach described in the previous section consists of the estimation of $V_p(t)$, IRR and $w(\tau)$. Equations described in the previous section will be used for the estimation of the variables.

To illustrate these calculations, first a demonstration will be done based on the simple synthetic model. Then it will be applied to the field production data. Methodology described over here is model free and is developed completely from the data.

4.2.1 Synthetic case: single fracture

Here for synthetic case a very simple model of single infinite conductivity fracture in a homogeneous reservoir is taken. Model used here is 'tartan' grid for a shale gas reservoir. It is a single hydraulic fracture. The fracture is fully completed i.e. completely penetrates the reservoir. The mesh size is $241 \times 189 \times 21$. The grid size is uniform in X and Z directions, i.e. DX = DZ = 10ft. In Y direction the grid size is logarithmic near the fracture. Minimum DY is 0.2 inch which is fracture width and maximum DY is limited to 50 ft. The reason for this is to provide better resolution near the fracture. Initial gas viscosity and compressibility are 0.03 cp and $1.212 \times 10^{-4}\, psi^{-1}$. The well is placed at the center of this single fracture and is produced with a constant bottom-hole pressure of 1000 psi.

Table 3 Parameter for single infinite conductivity fracture

Parameter	**Value**
Reservoir size	2410×2000×210 ft^3
Initial pressure	5470 *psi*
Bottom-hole pressure	1000 *psi*
Matrix porosity	0.046
Matrix permeability	0.0001 *mD*
Hydraulic fracture porosity	0.046
Hydraulic fracture permeability	1000 *mD*
Hydraulic fracture width	0.2 *in.*
Hydraulic fracture half-length	400 *ft*

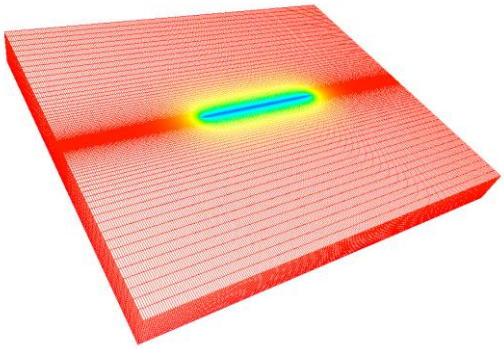

Figure 27 Single fracture on tartan grid and pressure distribution at 1000 days

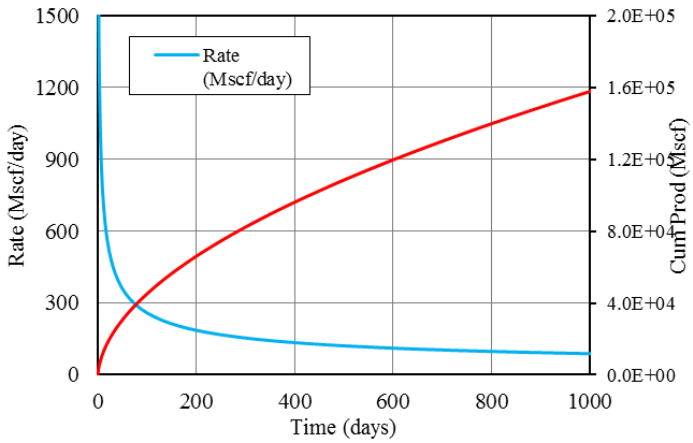

Figure 28 Production rate and cumulative production for the single fracture model (1000days)

This grid model was simulated with a commercial simulator (Eclipse). The rate and cumulative production are shown in the previous Fig.28. For showing varying effects, the model is simulated for a very long time i.e. 1.2E+05 days. In an actual field such a long production will not occur.

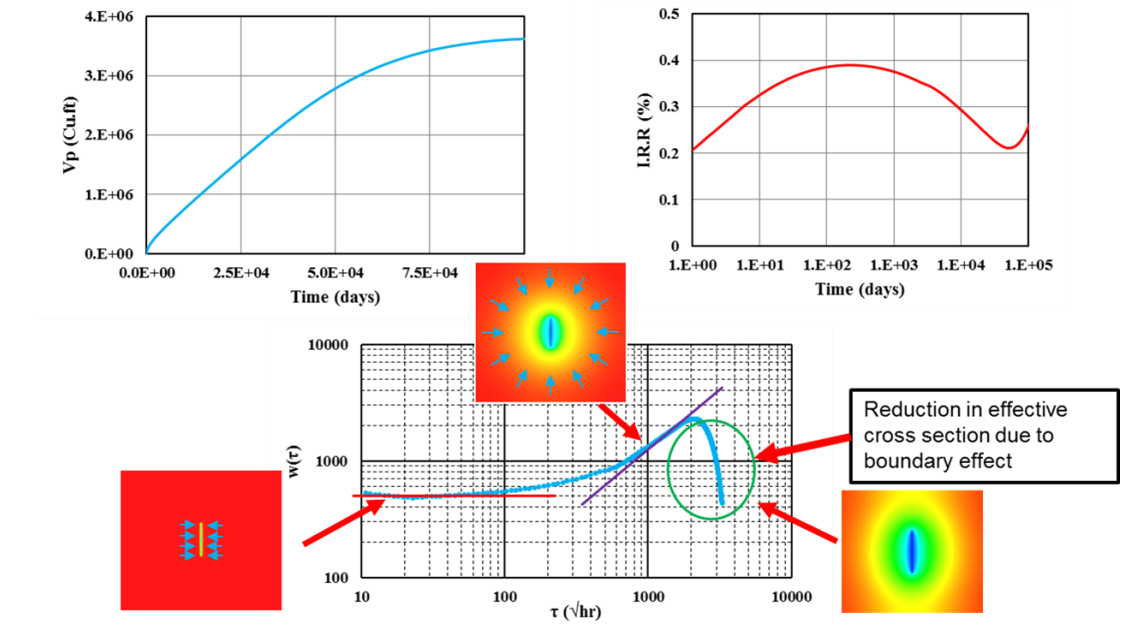

Figure 29 Analysis results for single fracture model: a) Drainage volume; b) I.R.R curve; c) w(τ) function

From the equations and methodology described in the earlier section, drainage volume, IRR and $w(\tau)$ functions were calculated as shown in the previous Fig. 29. We already know that the flow regime is going to be linear flow, then radial and then boundary dominated flow. From our analysis we can see these regimes very clearly.

For linear flow we know that the cross section for the flow is the fracture area through which the flow occurs and that the drainage volume will increase proportionally with the square root of time. In the $w(\tau)$ perspective we know that for the linear part we will have a value which is constant and it actually signifies the effective area of the fracture.

For radial flow regime the drainage volume is proportional to time and at the same time $w(\tau)$ is proportional to τ. This is clearly seen in the $w(\tau)$ plots of Fig. 29c.

At the very late time when our pressure wave hits the boundary, our drainage volume reaches the pore volume of the reservoir and effective cross-section for the flow should reduce to zero. This could be seen here as our drainage volume plot fall down towards the end. $w(\tau)$ plot shows sudden downfall in the end when boundary is hit by the pressure wave.

The IRR plots shown are on the semi-log axes. Early time recovery reaches a maximum value. This maximum value occurs when there is a shift from the linear flow to the radial flow. IRR is ratio of the production to the drainage volume. It gives us the view of how fast is the production done compared to the speed of drainage volume expansion. The increase in IRR initially is because of the fact that our flow regime is linear and production is at a much faster rate than the rate at which the drainage volume is increasing. But in the later stage, once the drainage volume starts expanding radially, our production speed is much less than that of the drainage volume expansion. Once the boundary has been hit then our drainage volume reaches the ultimate value, i.e. the pore volume. Then our IRR will keep on increasing as our production increases.

4.2.2 Field case application

Field case is not the same as the synthetic model. In the field case we have many irregularities in the production data. There are many shut downs and in addition, the flow rate and pressure are not very smooth like they are in the synthetic case. For application to the field production data we need to smooth the data and then apply the methodology. The procedure for application is explained in the next subsection.

4.2.2.1 Field application procedure

Field production data is very discontinuous in nature. While applying this methodology it is required to take the derivatives. Also for such data the derivatives calculation is not very easy and does not yield reasonable values. Thus the drainage volume and IRR estimation cannot be done directly. The variations in the data may be due to planned or unplanned shutdowns. Our procedure resolves this issue by neglecting build-up data and by taking derivatives with respect to the cumulative produced volume, rather than working in time. More smoothing of the data is required so that the outliers can be removed. This smoothing can be done either by local linear estimation in span throughout the data or by directly fitting a function which captures the trend of BHP and production rates. For unconventional reservoirs initial time period of 18 months is the most important data and this data conveys a lot about the reservoir behavior. Usage of cumulative production instead of time for smoothing will capture trends about the data and reservoir behavior.

For illustration let's see what happens when we do not apply the procedure for smoothing and directly calculate derivative from the data. Here we are calculating the derivative in two ways.

1. $$c_t \frac{d\Delta p_{wf}(t)}{q_w(t)dt} \approx \frac{1}{V_p(t)}$$

2. $$c_t \frac{d\left(\frac{\Delta p_{wf}(t)}{q_w(t)}\right)}{dt} \approx \frac{1}{V_p(t)}$$

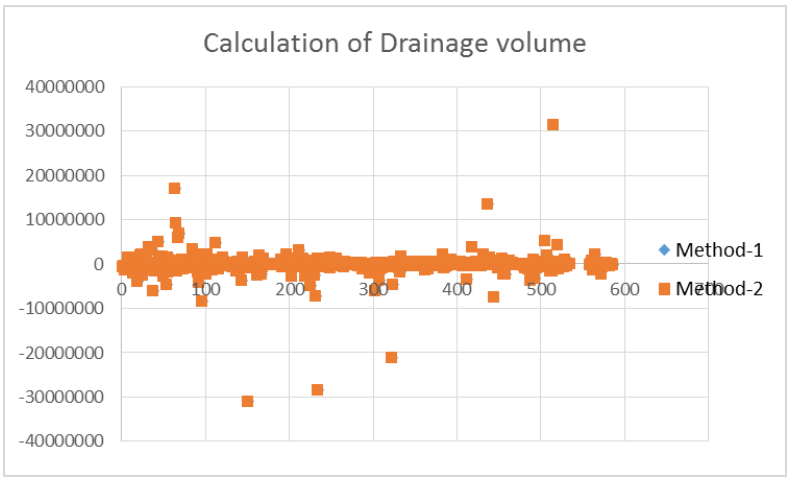

Figure 30 Drainage volume calculation without smoothing

In Fig. 30 we can see that if we do not pay attention to the shutdowns and irregularities in data then we are not able to capture any trend.

Now, a step by step procedure using data from one of the gas wells of Canada area is shown. This is just to show the steps of the analysis procedure. The next part after this will be the analysis for the two fields and subsequently the results will be discussed.

Here is the step by step procedure for analysis.

Step-1: Calculate cumulative production from the data

Well production data consists of production rate and surface pressure. Cumulative produced volume is used instead of time as explained earlier. So we need to calculate the cumulative produced volume at every time point which will account for the shut-in and the variable production rates.

Step-2: Bottom Hole Pressure calculation

Surface pressure requires to be converted to the bottom-hole pressure (BHP). This is done by pressure drop calculation throughout the vertical length of the well. Tubing pressure and production rate data is used for performing this calculation. These calculations are done based on the calculations shown in Chapters 6 & 7 of the Petroleum Production Systems .

Step-3: Calculation of Adjusted pressure (for gas wells, only)

For gas production, we will be using the pseudo pressure for analysis. Pseudo time and pseudo pressure need to be calculated. The calculation is based on the following equations:

$$P_a = \frac{\overline{\mu_g}.\overline{Z_g}}{\bar{P}} \int_0^P \frac{P.dP}{\mu_g Z}$$

$$t_a = \left(\overline{\mu_g}\overline{c_t}\right) \int_0^t \frac{dt}{\mu_g c_t}$$

Step-4: Smoothing of data for adjusted BHP

BHP and Production Rate are plotted against the cumulative produced volume. This data is fitted with a smooth curve with sufficient number of points to capture the trend of the data. The important point here is to get the trend of the data in the smoothed curve. In Fig. 32 the data points selected and not selected both are shown in different colors.

Step-5: Calculation of Drainage Volume, and I.R.R

The smooth curve fit is used to represent the adjusted pressure for data analysis. The derivative for the smoothed curve is calculated to get the drainage volume and IRR.

Step-6: Calculation of $w(\tau)$ function

Drainage volume calculated in the previous step gives us the data of drainage volume vs time. From this data the $w(\tau)$ function can be calculated as described previously.

Following plots show steps of the procedure:

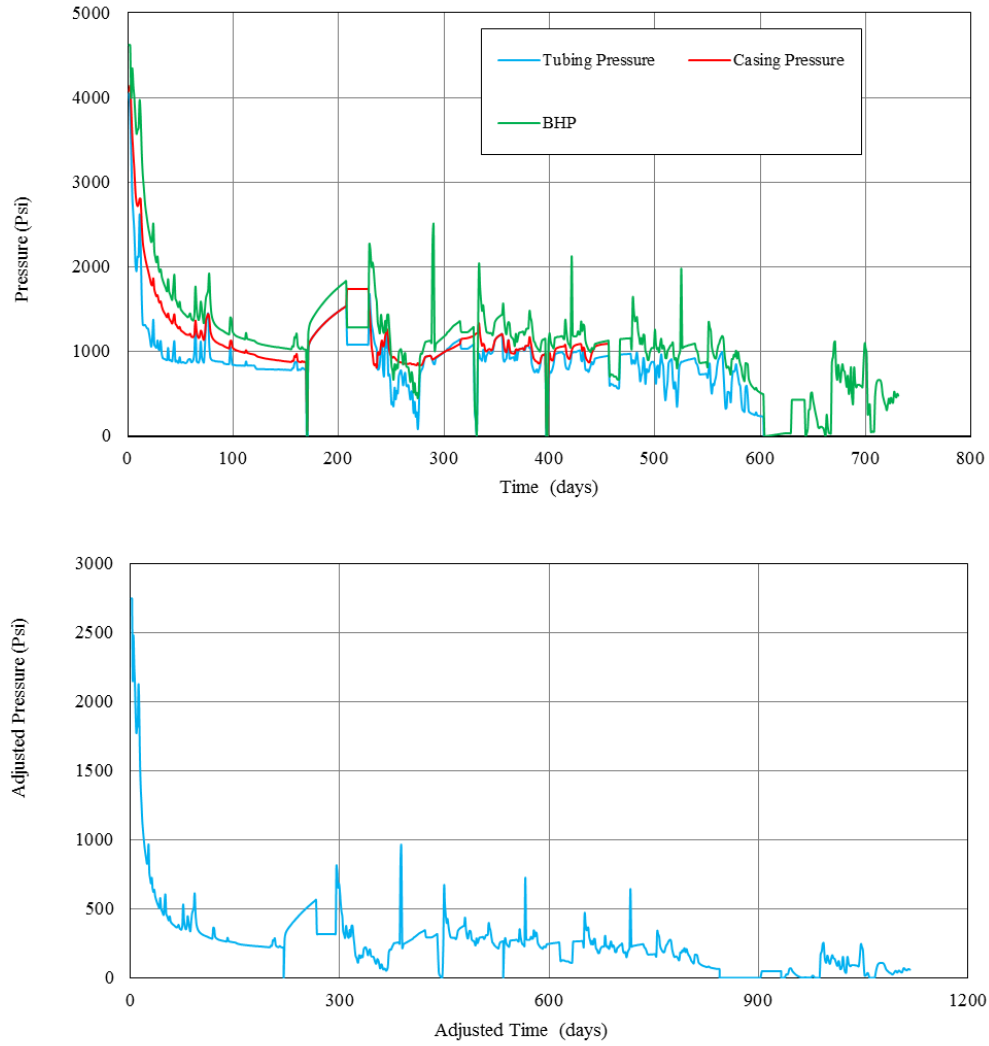

Figure 31 a) Pressure versus time; b) Adjusted pressure versus adjusted time

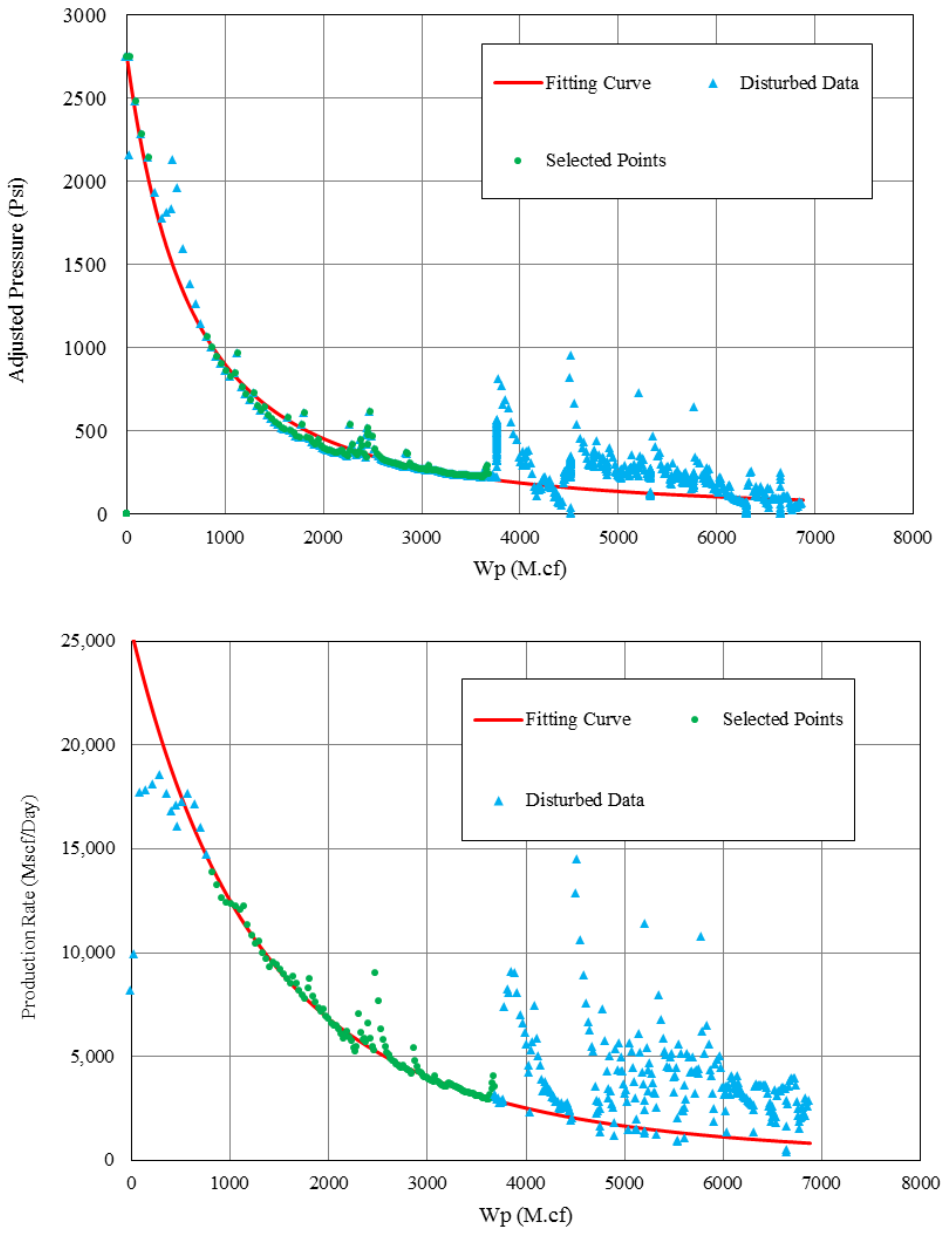

Figure 32 a) Adjusted pressure versus cumulative production Wp b) Production rate versus cumulative production Wp

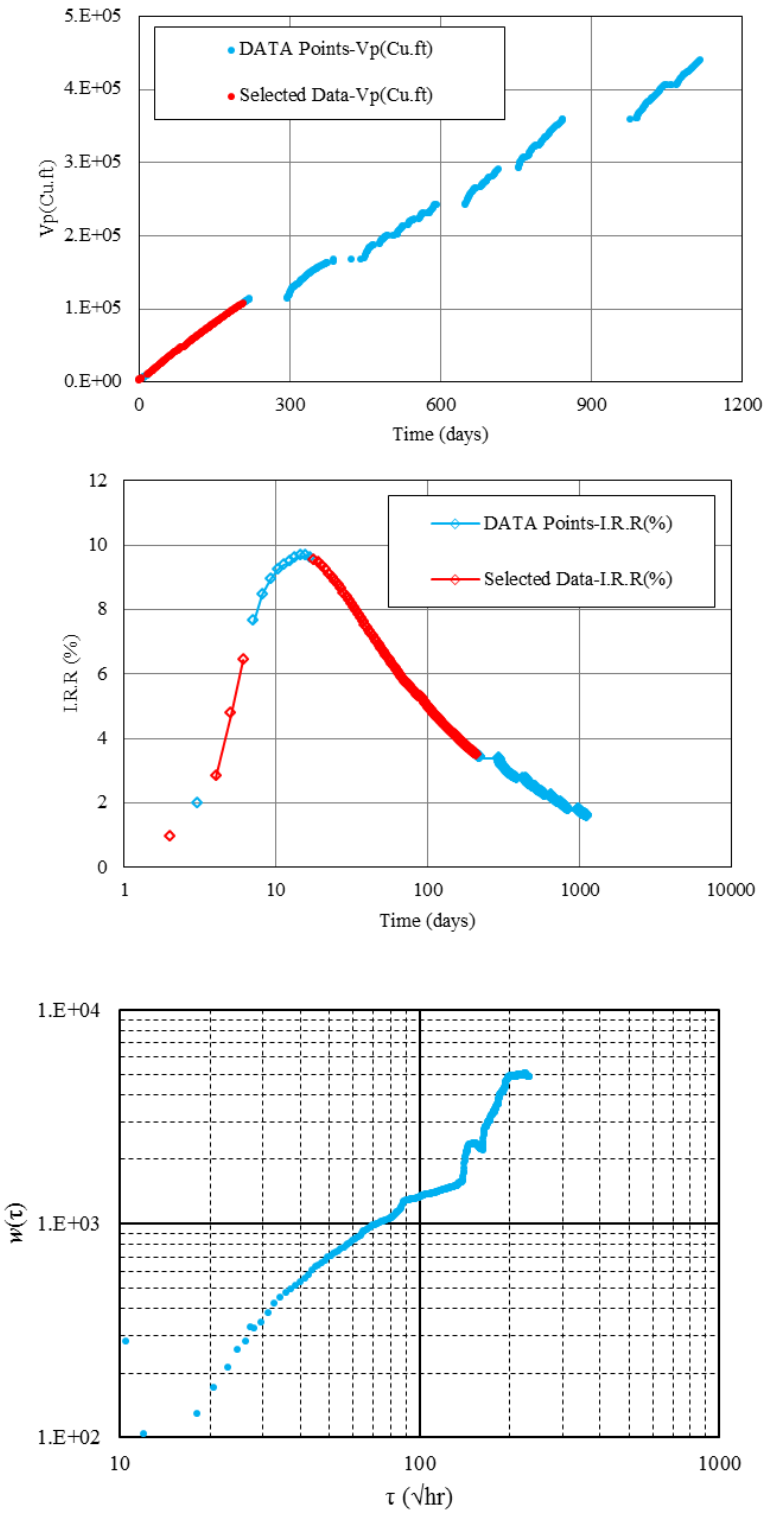

Figure 33 a) Drainage volume; b) I.R.R curve; c) w(τ) function

4.2.2.2 Field cases

Here an analysis technique which was discussed earlier is applied to two field data sets. First one is the data from a gas field and second one is the data from an oil field. Following are the two field data applications:

4.2.2.2.1 Field 1: application to shale gas production analysis

Description of the Field

Gas wells under consideration are the wells from the field which is located in the Lower Halfway River (LHR) basin in British Columbia, Canada. Porosity of the rock is 4.5%, permeability range given by the operator is 100-5000 nd, initial reservoir temperature 190 ^{o}F, initial reservoir pressure is about 4630 psi and formation thickness 200ft.

Table 4 Fixed parameters for the gas field.

Fixed Parameter	Value
Porosity	0.045
No. of Fractures	30
Initial Res. Pressure	4620 psi
Res. Temperature	190 °F
Lateral Length	5000 ft
Sw	0.25
Net Pay	200 ft

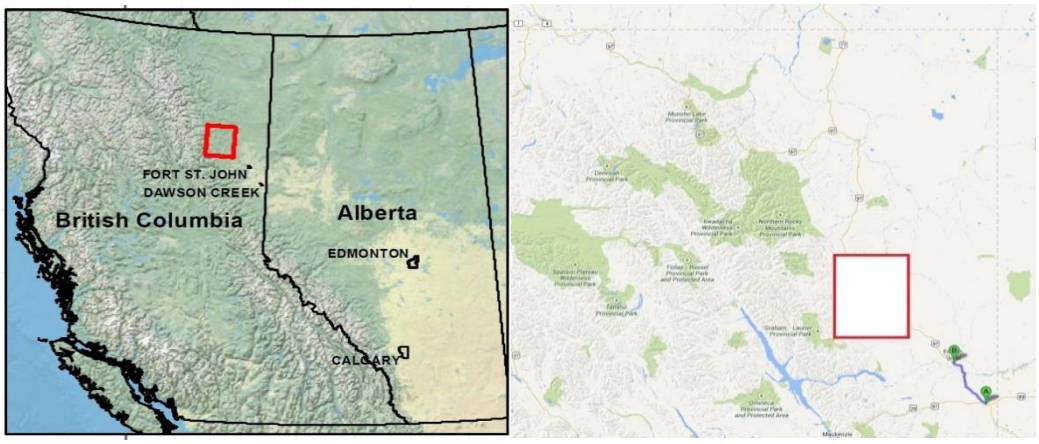

Figure 34 Geographic location of field

For this gas field we have the production data for 2 gas wells, named as 1D and 2D. Production history of the wells is shown below. The production history consists of the surface pressures (tubing and casing) and flow rates.

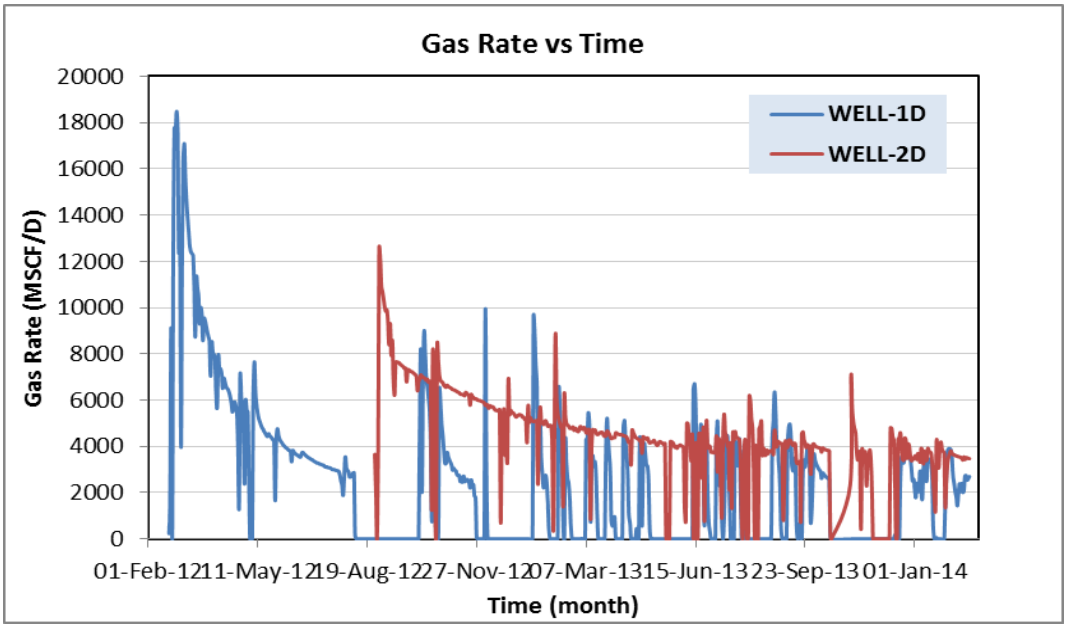

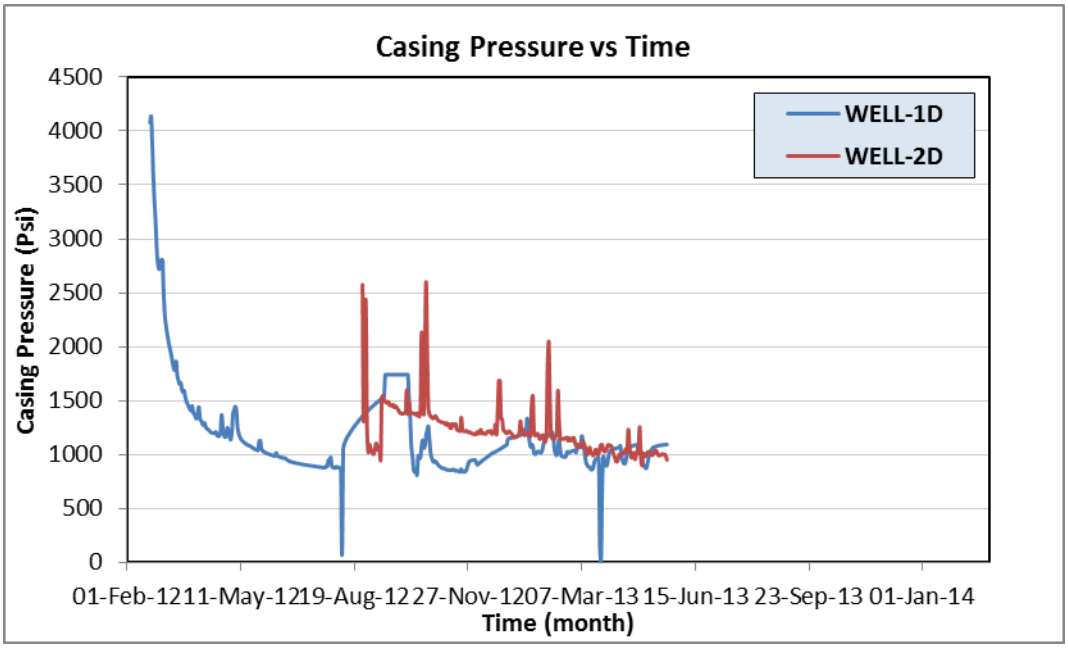

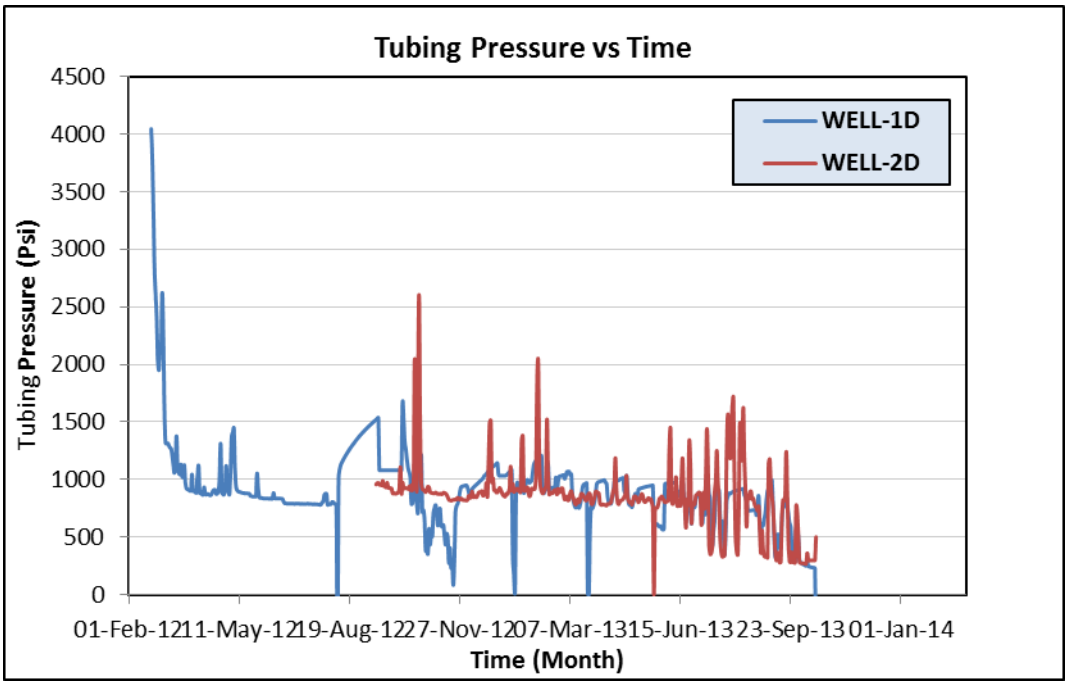

Figure 35 Production data (a) Gas rate (b) Casing pressure (c) Tubing pressure

From the field data the BHP of the well is calculated.

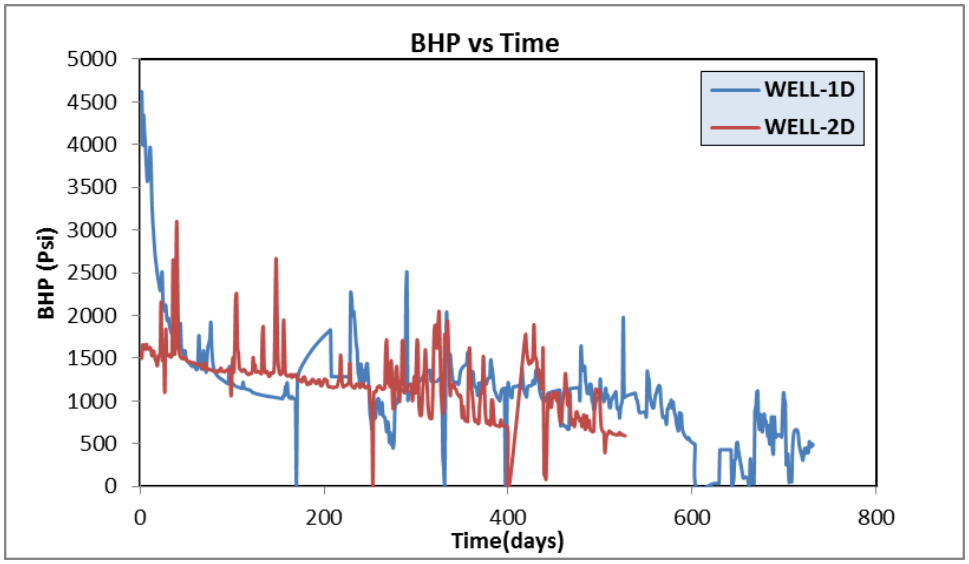

Figure 36 BHP vs time

Since the fluid is gas, so we need to deal with the pseudo pressure or adjusted pressure and time.

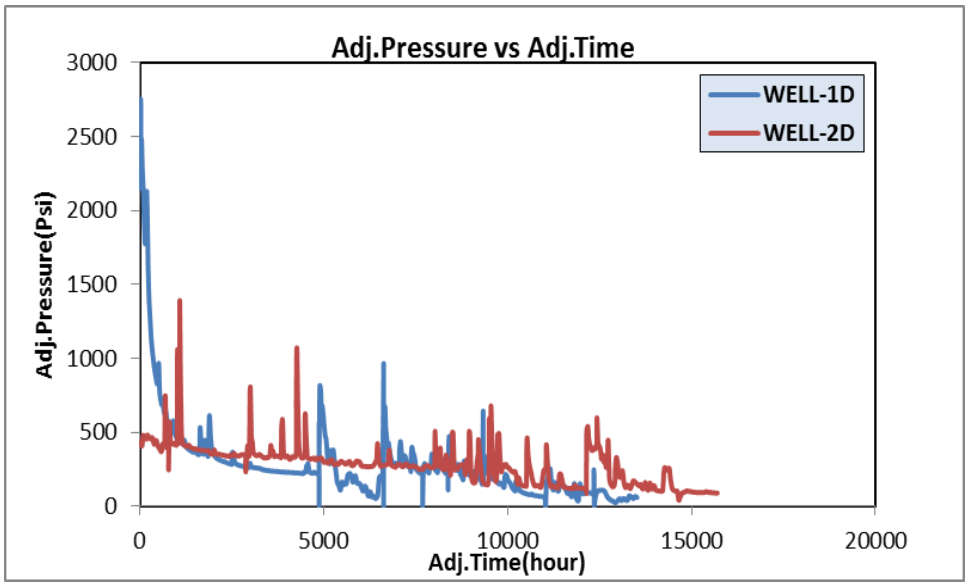

Figure 37 Adjusted pressure vs adjusted time

In Fig. 38 we show the results calculated according to the earlier mentioned method for the two different gas wells, Well-1D and Well-2D.

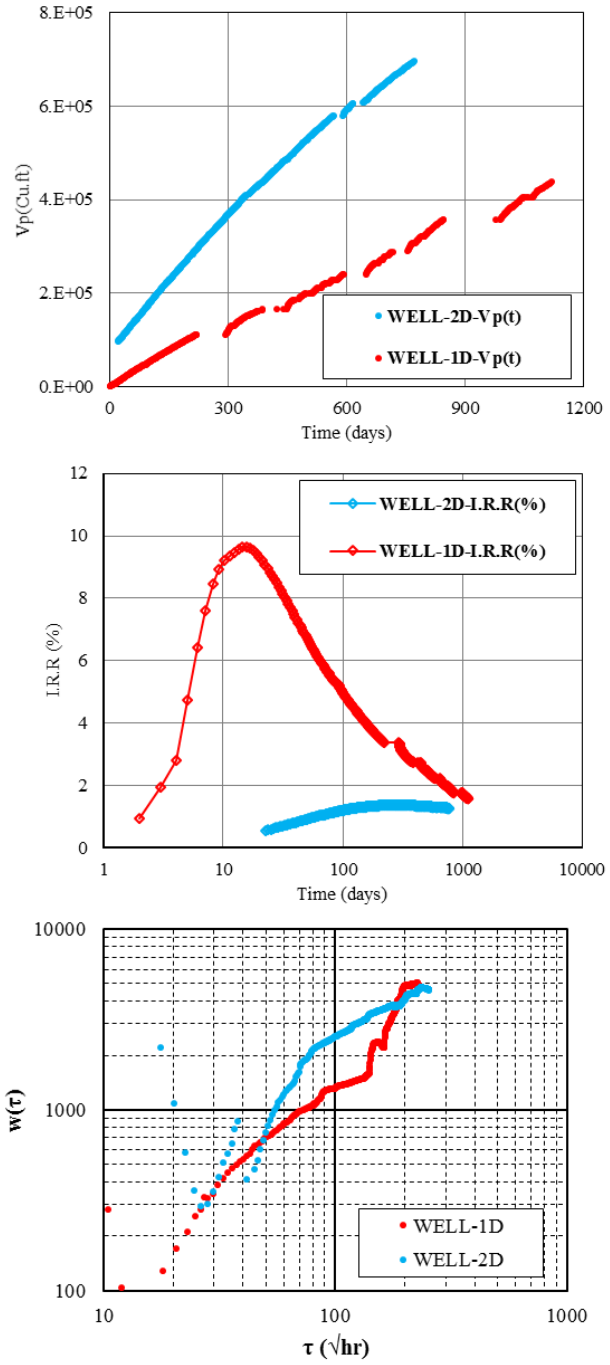

Figure 38 Analysis results for well-1D and well-2D: a) drainage volume; b) I.R.R curve; c) w(τ) function

Over here we can see from the drainage volume plot that Well-2D has better drainage characteristics. Although Well-1D has been flowing for a long time, still the expansion of the drainage volume for Well-2D is higher than Well-1D. Observation of drainage volume plot gives the overall picture but it would be more interesting if we put our observation window to other plots.

Further details can be seen in $w(\tau)$ plots. At early τ, both curves have similar values of $w(\tau)$, which indicates similar fracture areas. Moreover both the wells show faster than linear increase. $w(\tau)$ is derivative of drainage volume with spatial coordinate, so linear increase indicates radial flow and quadratic increase indicates spherical flow. An intermediate trend may indicate a partial completion with the drainage volume increasing both vertically and laterally. For late τ, both curves have similar values of $w(\tau)$, which again indicates similar drainage area at late time. For intermediate values of τ, Well-1D shows a linear trend while Well-2D is expanding more rapidly. Eventually Well-2D shows linear trend for radial flow, but consistently has larger values for $w(\tau)$. There can be various reasons for such trends such as partial completions, three dimensional flow or interference between the faults.

When we see IRR curve, it shows different trends for the wells. Well-1D has lower increase in drainage volume than Well-2D, for the production taken out of the well. Thus IRR value of Well-1D is higher as production/ drainage ratio is much more as compared to the Well-2D. It reached maximum value for Well-1D as soon as the drainage volume expansion increases faster than the production taken out. While for Well-2D the drainage volume is expanding in three dimensions and expansion is at a much faster rate than the production,

but at later stage when drainage volume is expanding in 2 dimensions (i.e. laterally) then the IRR curve reaches its peak.

4.2.2.2.2 Field 2: application to shale oil production data from the Eagle Ford field

Description of the field

Wells that are considered here are from the Eagle Ford field. There are 8 wells which are included within the analysis. The depth of the wells is approximately 11,000 ft. Initial reservoir pressure is 8,125 psi, temperature is 270 ^{o}F, porosity is 8.2% and permeability is in the range of 100-2,000 nD. The flow is mainly of oil with some gas and water. All fluids are converted to reservoir conditions and all phases are combined to get the production in reservoir barrels[30].

Table 5 Fixed parameters for the Eagle Ford field.

Fixed Parameter	Value
Porosity	0.082
No. of Fractures	20-22
Initial Res. Pressure	8125 psi
Res. Temperature	270 oF
Lateral Length	11000 ft
So	0.4

For this field we have the production data for 8 oil wells, named as 1H-4H and 9H-12H. The production history consists of the surface pressures (tubing and casing) and flow rates.

BHP for the well is also calculated based on pressure drop calculation for the fluids. All components of the fluid were combined together to get the overall properties of the fluid. Friction loss is calculated based on these properties of the fluid and the available well data.

Primary fluid from the data is oil, and BHP is calculated by adding the pressure drop to the tubing head pressure. The data points where tubing pressure in not available are considered as unavailable data points.

Table 6 Data for the BHP calculation

Data for BHP Calculation	
Casing Diameter (inch)	2.441
Depth (ft)	11100
Viscosity _oil (cp)	0.327
Density _oil	0.659
Viscosity_water (cp)	1
Density_water	1
Roughness	0.0006

Fluid recombination is described over here.

Total fluid volume: $V_{liq,res} = V_{o,res} + V_{g,res} + V_{w,res}$

Oil volume: $V_{o,res} = V_{o,std} B_o$

Gas volume: $V_{g,res} = V_{g(free),std} B_g = (V_{g,std} - V_{o,std} R_s) B_g$

Water volume: $V_{w,res} = V_{w,std} B_w$

Total: $V_{liq,res} = V_{o,std} B_o + (V_{g,std} - V_{o,std} R_s) B_g + V_{w,std} B_w$

Pressure drop is calculated based on the following equations and assumptions:

Viscosity and density for the fluid are calculated based on the volumetric weights.

Potential pressure drop: $\Delta P = \rho . g . l$

Frictional pressure drop: $\Delta P = \frac{2.f_f.\rho.u^2.l}{D}$

Where f_f is friction factor, $f_f = \frac{16}{N_{Re}}$, $N_{Re} < 2100$

$\frac{1}{\sqrt{f_f}} = -4\ log\left\{\frac{\epsilon}{3.7065} - \frac{5.0452}{N_{Re}} log\left[\frac{\epsilon^{1.1098}}{2.8257} + \left(\frac{7.149}{N_{Re}}\right)^{0.8981}\right]\right.$, turbulent

BHP for the 8 wells is calculated and production data is plotted with the cumulative production for each well.

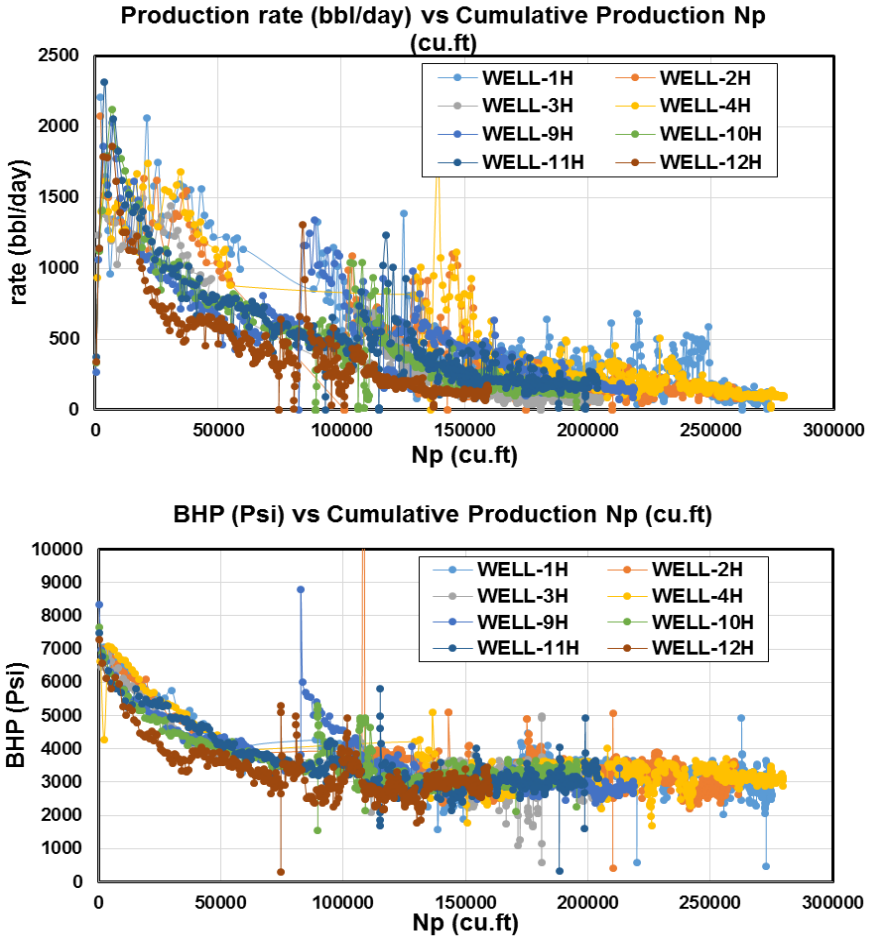

Figure 39 Production history of 8 wells 1,2,3,4 H and 9,10,11,12 H

In above plots production rate and calculated BHP is plotted against the cumulative produced volume.

Next are the analysis plots for the wells according to the method described in earlier section.

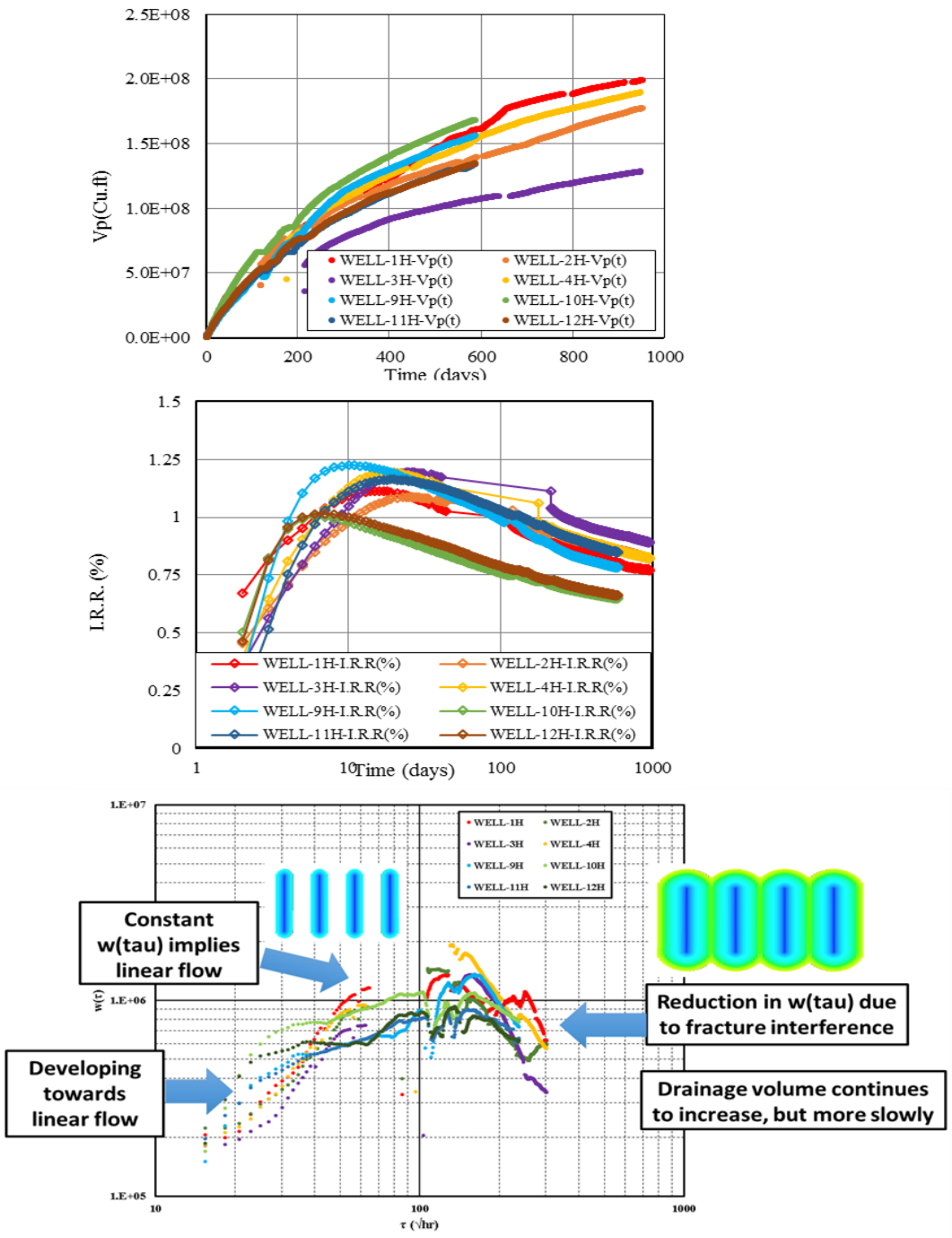

Figure 40 Eagle Ford well analysis (a) Drainage volume (b) I.R.R. curves (c) w(τ) function

For the above analysis of 8 wells, we have 3 plots (Fig. 40). When we see the drainage volume vs time plot we see a similar nature for all 8 wells. Drainage volume is increasing faster initially and starts to flatten up for later time. Possible reason could be the pressure wave is reaching to maximum value or a boundary effect. We can't reach to conclusion based on this.

IRR plots for 8 wells also show same type of nature. IRR reaches to maximum value and then start decreasing slowly. The reason for this is that drainage volume is not increasing at fast enough rate.

$w(\tau)$ plot for all 8 wells also have the same type of signature. It increases for small value of τ and then reaches to constant level and then starts decreasing for larger values of τ. Since $w(\tau)$ is dervative of drainage volume in spatial coordinate system τ which says that initially the drainage volume is increasing fast and then there is a constant increase and after that a small increase. This trend also supports drainage volume vs time plot.

If we directly do our analysis based on the data i.e. $w(\tau)$ plot , we can say that intially flow is developing towards linear, after that there is a constant area of wave propagation which is only possible when all fractures are acting separately. Once competition between fractures starts then there is decrease in $w(\tau)$ values. This is indicated in different region on $w(\tau)$ plot in Fig. 40 c.

Lets group some of the wells together i.e. WELL-11 and 12H; WELL-10 and 12H.

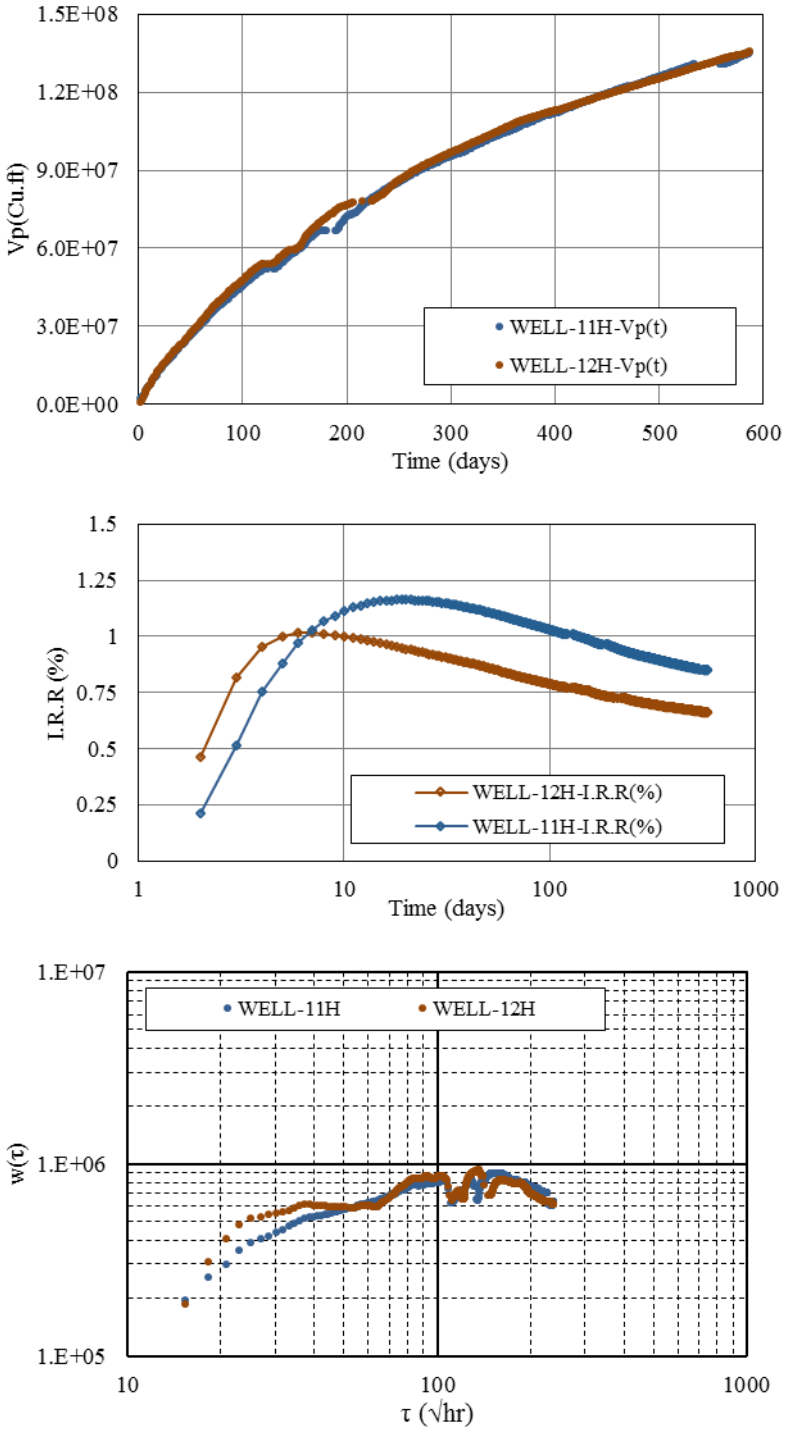

Figure 41 Analysis results for well-11H and well-12H: a) Drainage volume; b) I.R.R curve; c) w(τ) function

In Fig. 41 wells 11H and 12H are grouped together because they have similar response for drainage volume vs time i.e. Fig. 41a. When we see plot of $w(\tau)$ in Fig. 41c, we can notice that for 12H we have faster increase than 11H for initial τ values. For middle values of τ we have similar level of $w(\tau)$ for the two wells. The possible reason could be that the well 12H is partially completed and drainage volume is expanding very fast. This could be the reason why IRR for 12H reaches to maximum values much before than 11H.

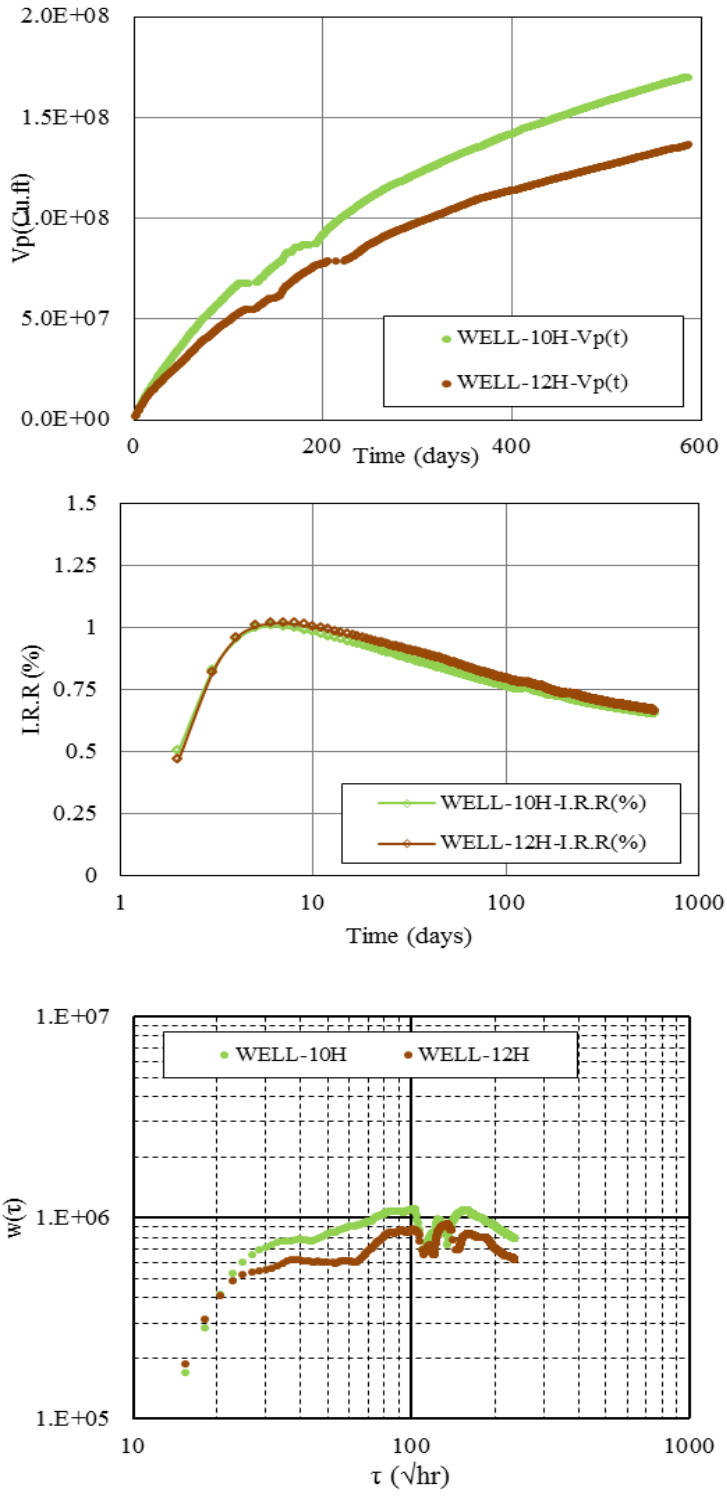

Figure 42 Analysis results for well-10H and well-12H: a) Drainage volume; b) I.R.R curve; c) w(τ) function

In Fig.42 wells 10H and 12H are grouped together. These wells are grouped together because they have similar response for IRR plot. Drainage volume vs time plot i.e. Fig.42a shows a big difference between the response of the two wells. Well 10H has higher drainage throughout the plot than 12H. $w(\tau)$ plots for the two wells also show that 10H has much higher $w(\tau)$ values than 12H which explains why drainage volume response for 10H is more than 12H. Hence we can infer that 10H well is more upscale version of 12H well.

5. CONCLUSION AND RECOMMENDATION

This thesis is focused on exploring the application of the methodology of the drainage volume. This methodology was further applied to derive the model based drainage volume curves for an infinite conductivity fracture. Apart from this application a novel approach for the analysis of production data for shale gas/oil reservoir was also explored and applied.

The main findings drawn from this research are summarized below:

- For transient flow in a reservoir, we have used the concept of Diffusive Time of Flight. Diffusivity equation is transformed into 1D in DTOF as spatial coordinate. This transformation accommodates the diffusivity information within the $w(\tau)$ function.
- The relationship between the pore volume in spatial coordinates $\left(V_p(\tau)\right)$ and the drainage volume in time $\left(V_p(t)\right)$ is useful for derivation of type curves. Three models were explored based on this relationship. The application of these models depends on whether we are dealing with early time or later time. The pill box model is applicable for early time and for later time all the models behave the same.

  But when dealing with the actual field data, we can safely say that we never reach to very late time scenarios. So the application of pill box model is justified for multiple fracture horizontal well.
- Our novel approach for analysis helps us to interpret the production data and evaluate the pressure wave geometry directly from production data (without any model) by evaluating

- Drainage Volume vs Time
- Instantaneous Recovery Ratio vs Time
- Drainage Volume Geometry: $w(\tau)$

The drainage volume gives a description of how fast the drainage is growing with the time but it does not give a description of the geometry of the drainage volume in spatial coordinates. This information is obtained from the plot of $w(\tau)$. The IRR curve gives a strong indication of the change in the flow. All the three plots give a better insight to the flow behavior when looked together.

- Drainage Volume curve and $w(\tau)$ could be used for estimation of the properties of the fracture and reservoir. This will require a model for fitting the data and needs to be explored further in future research.
- Our new method works on the basic equation for a fixed flow rate production from a well. However, in the field, the slowing of instantaneous flowrate is the case. This assumption is not adequately justified and should be explored further in future research. However deconvolution technique can be explored but it also requires data smoothing.
- The smoothing technique which is used over here is fitting a smooth curve in order to catch the overall trend of the production data. More efficient techniques can be applied for the same.

REFERENCES

[1] petrowiki,http://petrowiki.org/images/b/b5/Vol5_Page_0786_Image_0001.png. Accessed date: 4.12.2016.

[2] Cinco-Ley, H. and F. Samaniego-V, Transient Pressure Analysis for Fractured Wells. Society of Petroleum Engineers, 1981.

[3] Blasingame, T.A., S. Amini, and J. Rushing, Evaluation of the Elliptical Flow Period for Hydraulically-Fractured Wells in Tight Gas Sands -- Theoretical Aspects and Practical Considerations, in SPE Hydraulic Fracturing Technology. 2007, Society of Petroleum Engineers.

[4] Arps, J.J., Analysis of Decline Curves. Society of Petroleum Engineers. , 1945.

[5] Fetkovich, M.J., Decline Curve Analysis Using Type Curves. Society of Petroleum Engineers, 1980.

[6] Valko, P.P. and W.J. Lee, A Better Way To Forecast Production From Unconventional Gas Wells, in Society of Petroleum Engineers. 2010, Society of Petroleum Engineers.

[7] Al-Kobaisi, M., et al., Pressure-Transient-Analysis of Horizontal Wells with Transverse, Finite-Conductivity Fractures, in Canadian International Petroleum Conference. 2006, Petroleum Society of Canada.

[8] Ilk, D., V. Okouma Mangha, and T.A. Blasingame, Characterization of Well Performance in Unconventional Reservoirs using Production Data Diagnostics, in Society of Petroleum Engineers. 2011, Society of Petroleum Engineers.

[9] Song, B. and C.A. Ehlig-Economides, Rate-Normalized Pressure Analysis for Determination of Shale Gas Well Performance, in Society of Petroleum Engineers. 2011, Society of Petroleum Engineers.

[10] Kulkarni, K.N., A. Datta-Gupta, and D.W. Vasco, A Streamline Approach for Integrating Transient Pressure Data Into High-Resolution Reservoir Models. Society of Petroleum Engineers, 2001.

[11] Vasco, D. and A. Datta-Gupta, Asymptotic solutions for solute transport: A formalism for tracer tomography. Water Resources Research, 1999. 35(1): p. 1-16.

[12] Nunna, K., P. Zhou, and M.J. King, Novel Diffuse Source Pressure Transient Upscaling, in Society of Petroleum Engineers. 2015, Society of Petroleum Engineers.

[13] Lee, J., Well Testing: New York: Society of Petroleum Engineers,Original edition. ISBN 0895203170,1982.

[14] http://physics.stackexchange.com/questions/1289/waves-in-water-always-circular, Accessed date: 4.12.2016.

[15] Yang, C., et al., A Novel Approach for Production Transient Analysis of Shale Gas/Oil Reservoirs, in URTeC. 2015, Society of Petroleum Engineers.

[16] Zhang, Y., et al., From Streamlines to Fast Marching: Rapid Simulation and Performance Assessment of Shale Gas Reservoirs Using Diffusive Time of Flight as a Spatial Coordinate, in Society of Petroleum Engineers. 2014, Society of Petroleum Engineers.

[17] Cheng, Y., W.J. Lee, and D.A. McVay, A New Approach for Reliable Estimation of Hydraulic Fracture Properties Using Elliptical Flow Data in Tight Gas Wells. Society of Petroleum Engineers, 2009.

[18] Gringarten, A.C., H.J. Ramey, Jr., and R. Raghavan, Unsteady-State Pressure Distributions Created by a Well With a Single Infinite-Conductivity Vertical Fracture. Society of Petroleum Engineers, 1974.

[19] Hale, B.W. and J.F. Evers, Elliptical Flow Equations for Vertically Fractured Gas Wells. Society of Petroleum Engineers, 1981.

[20] Kucuk, F. and W.E. Brigham, Transient Flow in Elliptical Systems. Society of Petroleum Engineers, 1979.

[21] Prats, M., Effect of Vertical Fractures on Reservoir Behavior-Incompressible Fluid Case. Society of Petroleum Engineers, 1961.

[22] Liao, Y. and W.J. Lee, Depth of Investigation for Elliptical Flow Problems and Its Applications to Hydraulically Fractured Wells, in Society of Petroleum Engineers. 1994, Society of Petroleum Engineers.

[23] Coats, K.H., M.R. Tek, and D.L. Katz, Unsteady-State Liquid Flow Through Porous Media Having Elliptic Boundaries. 1959, Society of Petroleum Engineers.

[24] Obuto, S.T. and T. Ertekin, A Composite System Solution in Elliptic Flow Geometry (includes associated papers 20800 and 21470). Society of Petroleum Engineers, 1987.

[25] Papatzacos, P., Exact Solutions for Infinite-Conductivity Wells. Society of Petroleum Engineers, 1987.

[26] Stehfest, H., Algorithm 368: Numerical inversion of Laplace transforms [D5]. Communications of the ACM 1970. 13(1): p. 47-49.

[27] Mathematica, W., http://www.wolframalpha.com/. Accessed date: 4.12.2016.

[28] Lee, J., Pressure Transient Testing, SPE. 2003. 9.

[29] http://www.itasca-image.com/services/Hydraulic-fracture-modelling, Accessed date: 4.12.2016.

[30] Michael J. Economides, A.D.H., Christine Ehlig-Economides, Ding Zhu, Petroleum Production Systems. 2012.